Technical White Paper

Determining the Low-Temperature Rheological Properties of Asphalt Binder Using a Dynamic Shear Rheometer (DSR)

Fundamental Properties of Asphalts and Modified Asphalts III Product: FP 08

March 2015

Prepared for
Federal Highway Administration
Contract No. DTFH61-07-D-00005

By
Mike Farrar, Changping Sui, Steve Salmans, and Qian Qin
Western Research Institute
3474 North 3rd Street
Laramie, WY 82072
www.westernresearch.org

WesternResearch
INSTITUTE

TABLE OF CONTENTS

LIST OF FIGURES

LIST OF FIGURES (continued)

LIST OF FIGURES (continued)

LIST OF FIGURES (continued)

LIST OF TABLES

DETERMINING THE LOW-TEMPERATURE RHEOLOGICAL PROPERTIES OF ASPHALT BINDER USING A DYNAMIC SHEAR RHEOMETER (DSR)

INTRODUCTION

The purpose of this report is to document the development of a new dynamic shear rheometer (DSR), low-temperature asphalt binder rheology method under FHWA Fundamentals Contract No. DTFH61-07-D-00005. The proposed oscillatory shear method is an alternative to the bending beam rheometer (BBR) which is currently in use by transportation agencies and asphalt research laboratories around the world.

The DSR is the critical apparatus used in the SuperPave performance-graded (PG) binder system for high and intermediate temperature. During the Strategic Highway Research Program (SHRP), DSR with parallel plate geometry, was considered for the low temperature PG system, but it wasn't selected because it was recognized that DSR mechanical measurements at temperatures below about 5°C produced substantial compliance errors in the absolute values of the dynamic moduli [$G'(\omega)$ and $G''(\omega)$] and relaxation modulus $G(t)$ [Christensen and Anderson 1992]. Instead, SHRP developed the BBR (AASHTO T 313) to measure the low temperature rheological properties of asphalt binder. The BBR does not suffer from instrument compliance error.

The limiting temperature of about 5°C for DSR parallel plate measurements due to instrument compliance has been resolved by measuring the instrument compliance and performing appropriate corrections to the data. DSR measurements can now be made to as low as -40°C [Sui et al. 2010].

This report documents the resolution of the compliance issue and other related issues in order to develop an AASHTO/ASTM DSR method as an alternative to BBR. A draft method in AASHTO format is provided in the Appendix. The proposed method is titled "Standard Method of Test for Determining the Low Temperature Rheological Properties of Asphalt Binder Using a Dynamic Shear Rheometer (DSR)."

The DSR draft AASHTO test method involves the determination of the dynamic moduli of asphalt binder when tested in dynamic (oscillatory) shear using parallel plate test geometry at low (-40 to 5°C) temperature. The test method is intended for determining the linear viscoelastic properties of asphalt binders as required for specification testing.

The method allows the use of 4 and 8 mm diameter parallel plates at low temperature. During the initial method development, 4 mm diameter plates were used and the method was referred to as "4-mm DSR." Later on, 8 mm diameter plates were included in the method. Although the method allows both 4 and 8 mm diameter plates, the method will be referred to hereinafter as simply "4-mm DSR."

To determine BBR m-value and creep stiffness S (t), from 4-mm DSR data, a correlation was developed by Sui et al. [2011]. In this method, the slope and magnitude of the shear stress relaxation modulus $G(t)$ master curve at 2 hours and at the true low PG grading temperature are correlated with the corresponding $S(t)$ and m-values at 60 seconds and 10°C above the true low PG grading temperature from BBR measurements.

Just as the BBR test temperature and creep time were modified from the PG test temperature and two hours to the PG temperature plus 10°C and 60 seconds, the Sui et al. method has been recently modified by measuring $G(t)$ slope and magnitude at 60 seconds and 10°C warmer than the PG grading temperature.

Four mm DSR only tests 25 mg of material (in practice about 150 mg is necessary in order to allow sample trimming, etc.), which is several orders of magnitude less than the amount required to fabricate a BBR beam. Also, no specimen pre-molding is needed and a relatively low temperature (60 ~ 70°C) is required to load the samples into the rheometer.

This report demonstrates 4-mm DSR is a reliable, rapid test for the acquisition of low-temperature rheological properties of asphalt binder and other asphaltic materials such as emulsion residue and crack sealant that experience low temperatures in the field.

Background

A dispute concerning the modulus of glycerol in the glassy regime (G_g) led Schröter et al. [2006] to develop a method to correct for the compliance of a dynamic shear rheometer, and its tools and platens. Sui et al. [2010] applied this compliance correction method to asphalt binder low temperature dynamic shear measurements (~ 5°C to -40°C) using 4 mm diameter parallel plates and a 1.75 mm gap. The effect of the compliance correction is demonstrated in figure 1. At low frequency (high temperature) the asphalt binder is compliant and the effect of instrument compliance is negligible. However, at high frequency (low temperature) the asphalt binder is no longer compliant and the effect of instrument compliance is significant. Instrument compliance correction adjusts the DSR measurements to reveal the true magnitude of the bitumen glassy modulus.

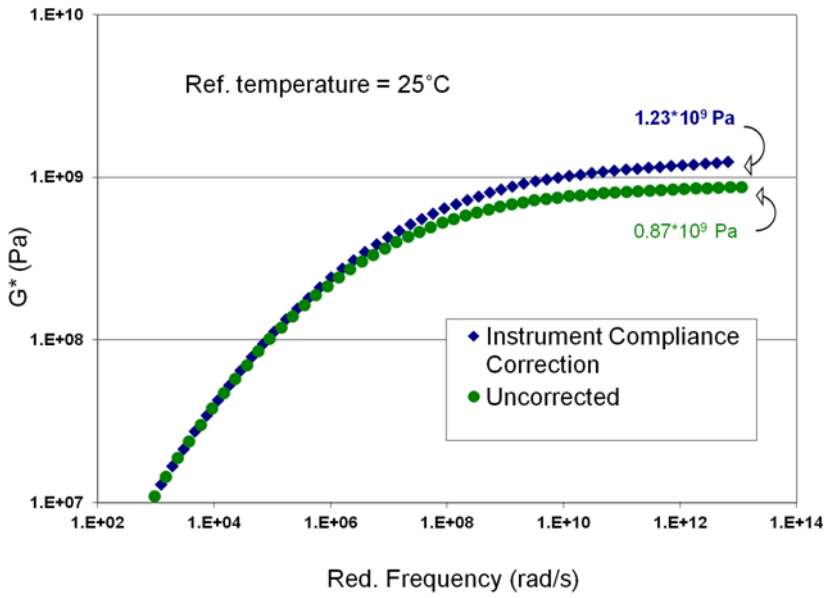

Figure 1. Graph. 4-mm DSR – Aged asphalt binder, complex shear modulus master curves from corrected and uncorrected data.

4-mm DSR Spinoffs

Figure 2 displays a number of new and novel 4-mm DSR spin-off technologies and applications that are under development at WRI. These include:

- A DSR alternative to BBR [Sui et al. 2010, Sui et al. 2011, this technical white paper].
- USAT- Universal Simple Aging Test. An alternative to the rolling thin film (RTFO) test and standard PAV test methods and associated specifications for HMA and WMA [Farrar et al. 2015a, Farrar et al. 2014a, Farrar et al. 2012].
- Laboratory emulsion recovery, oxidative aging, and testing. [Farrar et al. 2013a, Salmans et al. 2015, Farrar et al. 2014b].
- Asphalt pavement Micro-Sampling and Micro-Extraction [Farrar et al. 2015b].
- Low temperature properties of Sasobit modified WMA [Qin et al. 2015, Qin et al. 2014a, Qin et al. 2014b].

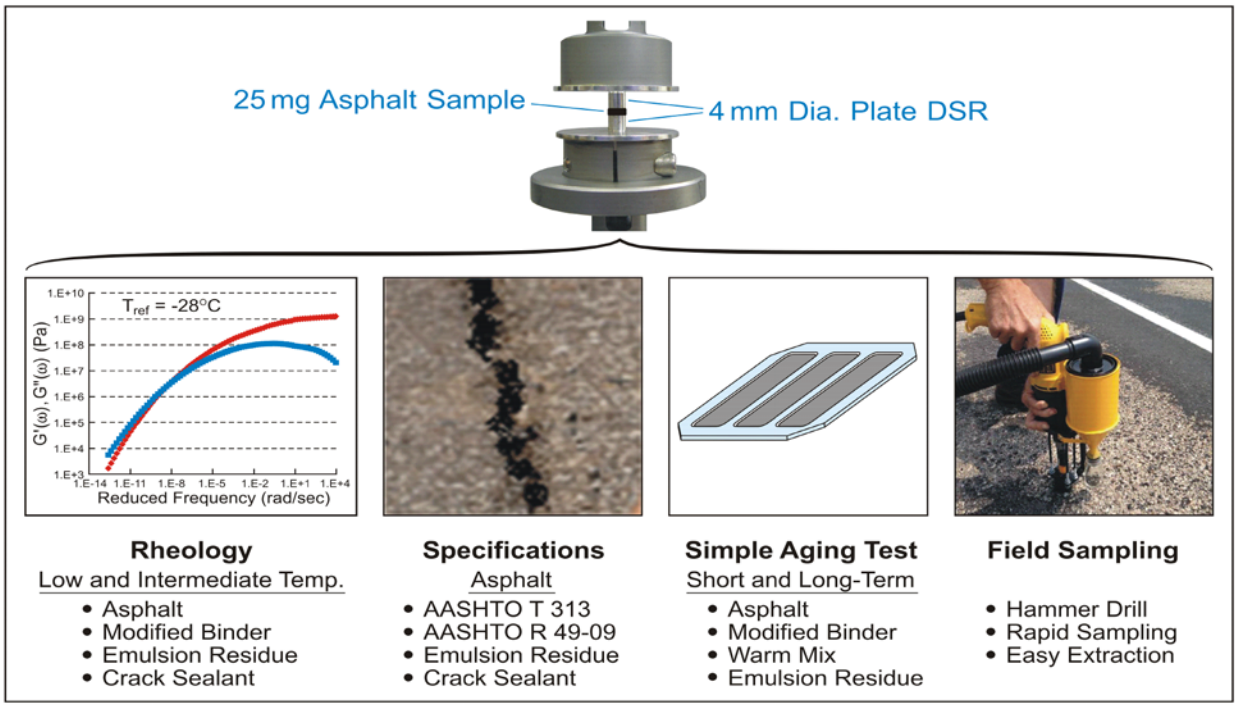

Figure 2. Diagram. Four-mm DSR spin-off technologies.

EXPERIMENTAL

Dynamic shear moduli determinations, and stress relaxation and creep measurements were performed with three Malvern Kinexus controlled stress dynamic shear rheometers, a TA Instruments ARES controlled strain dynamic shear rheometer and an AR-G2 controlled stress dynamic shear rheometer. The potential testing temperature range for the 4-mm DSR is from -40 to +60°C. The actual range depends on the stiffness of the binder. For example, RTFO and RTFO/PAV aged paving grade asphalts can typically be tested to -30°C and in some cases -40°C. Whether or not reliable data at -40°C can be achieved depends on the glassy modulus temperature. The glassy modulus is generally considered as 1 GPa for paving grade asphalts. On the upper end, reliable frequency sweep data can generally be obtained at 30°C and in some cases as high as 60°C. The key to the upper limit is sufficient binder stiffness to generate measurable torque.

Asphalt binders were annealed in an oven at 70°C to eliminate steric and physical hardening. The annealed asphalt binders are then transferred directly to the lower fixed plate (preheated to 50-60°C) using a metal spatula or similar tool. No pre-molding is used.

The Kinexus and AR-G2 rheometers environmental control systems included a circulating fluid bath and Peltier plates to maintain temperatures near and below ambient. The ARES environmental control system included a liquid nitrogen assembly to maintain temperatures near and below ambient.

BBR was performed in accordance with AASHTO T 313.

RESULTS AND DISCUSSION

The following discussion covers the laboratory test results generated over several years to allow WRI to develop an AASHTO/ASTM standard method for 4-mm DSR. The draft standard in AASHTO format is provided in the Appendix.

Concept of Machine Compliance and Its Correction

When the true shear strain applied is significantly lower than the command strain because the sample/geometry configuration is stiff compared to the instrument, the test fixtures and the torque transducer are also deformed by the stress required to shear the sample. The deformation of the test fixtures and transducer constitutes the instrument compliance [Gottlieb and Macosko 1982]. Significant error in the reported mechanical properties may result if the compliance is not properly taken into account.

All materials will deform under load. In rheology, the deformation due to the compliance of instruments at low testing temperature is generally referred to as machine compliance or instrument compliance. Instrument compliance can lead to huge errors when measuring material properties near a material's glassy regime [Schröter et al. 2006; Mackay and Halley 1991; Hutcheson and McKeena 2008]. The reason is obvious with respect to the following equations (figures 3 and 4):

$$G = \frac{\tau}{\gamma}$$

Figure 3. Equation. Shear modulus.

$$\gamma_{measured} = \gamma_{sample} + \gamma_{instrument} = \frac{\tau}{G_{sample}} + \frac{\tau}{G_{instrument}}$$

Figure 4. Equation. Measured strain.

In these equations G is the modulus, τ is the stress, and γ is the strain. At high temperatures, i.e., temperatures well above the glass transition of the sample, the modulus is low and is much less than that of the instrument or measuring tool (stainless steel or aluminum), the deformation due to the machine compliance or the second term in the right hand side of figure 4 is negligible. Consequently, the measured modulus is the actual modulus of tested material. However, at low temperatures or temperatures close to and below the glass transition temperature of the sample, the modulus becomes close to that of the instrument or measuring tool. In this case, the compliance from the instrument, second term on the right hand side of figure 4, is not negligible. As a result, the measured modulus of the sample is lower than its true value. This can lead to an error factor of approximately ten in the estimation of the glassy shear modulus.

The machine compliance issue is common to all rheometers and has long been recognized in the polymer field. However, no systematic studies had been conducted to address the problem until the work of Schröter et al. [2006], Hutcheson and McKenna [2008], and Hutcheson [2008].

Following is a summary of the machine compliance correction from Schröter et al. [2006]. Figures 5 and 6 were used to correct for machine compliance error.

$$\frac{1}{K^*_{mes}} = \frac{1}{K^*_s} + \frac{1}{K_t}$$

Figure 5. Equation. Inverse torsional stiffness (compliance).

$$K = G\frac{\pi}{2}\frac{R^4}{h}$$

Figure 6. Equation. Torsional stiffness of a cylindrical sample.

where K^*_{mes} and K^*_s are the respective measured and actual complex torsional stiffnesses and K_t is the machine torsional (elastic) stiffness. G is the shear modulus of the material in torsion, h is the gap between the plates, and R is the radius of the plates. For viscoelastic materials like the sample, torsional stiffness is the complex modulus (G^*). G can be used for an elastic material like the instrument. Figure 5 states that the measured compliance (deformation) is the summation of the compliances of sample and instrument. Substituting figure 6 into figure 5, one obtains the following equation (figure 7):

$$\frac{2h}{\pi G^*_{mes} R^4} = \frac{2h}{\pi G^*_s R^4} + \frac{1}{K_t}$$

Figure 7. Equation. Measured compliance.

The instrument compliance correction involves both dynamic moduli $G'(\omega)$, and $G''(\omega)$ because the sample is a viscoelastic material and the complex inverse of torsional stiffness is a complex inversion [Schröter et al. 2006].

Measuring the Instrument Compliance of a Dynamic Shear Rheometer, Tools and Platens

After several attempts, Schröter et al. [2006] developed a method to accurately measure total instrument compliance including the plates. They machined a solid rod fixture with the same dimensions as if two disposable plates had been welded together as shown in figure 8. The solid rod geometry was then attached to the disposable plate holders, and the compliance was determined by varying the angular motor displacement and measuring the torque generated. Schröter et al. measured the machine compliance for the total system (note: they were working with an ARES rheometer) using 6 and 8 mm diameter rods, and the compliance values were .009761 and .008102 rad/Nm, respectively.

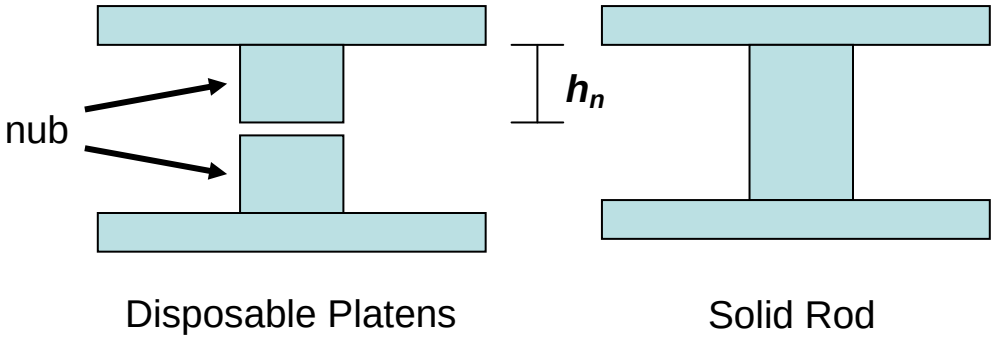

Figure 8. Illustration. A simple schematic showing the geometry of the solid rod and the disposable platens [from Schröter et al. 2006].

In the initial work at WRI, 4-mm diameter disposable aluminum plates (machined down from 8 mm diameter disposable plates) were used. The machine compliance for the 4-mm diameter parallel plates measuring system was calculated using the following equation (figure 9) (proposed by Schröter et al. [2006]).

$$\frac{1}{K_t} = \frac{1}{K_x} + 2\frac{1}{K_n}$$

Figure 9. Equation. Total compliance.

where $1/K_x$ is the compliance of the ARES and disposable plate holders, and $1/K_n$ is the compliance of one nub of the disposable plate.

From figure 6, one has:

$$\frac{1}{K_n} = \frac{2}{\pi G_n}\frac{h_n}{R^4}$$

Figure 10. Equation. Nub compliance.

where G_n is the shear modulus of the plate material (aluminum in our case for our ARES rheometer). G_n for aluminum is reported in the literature as 26 GPa [Jacobs and Kilduff 2001].

Using the above instrument compliance values reported by Schröter et al. for their ARES rheometer, the instrument compliance correction for WRI's ARES rheometer with 4-mm parallel aluminum plates was estimated as 0.02265 rad/Nm.

Instrument Compliance Measured with Solid Rod Fixture

Of course, one should be cautious in adopting machine compliance values from the literature. So to check the instrument correction (0.02265 rad/Nm) for WRI's ARES system (with aluminum plates) a solid aluminum rod, shown in figure 11 was machined with the same dimensions as the two platens adhered together.

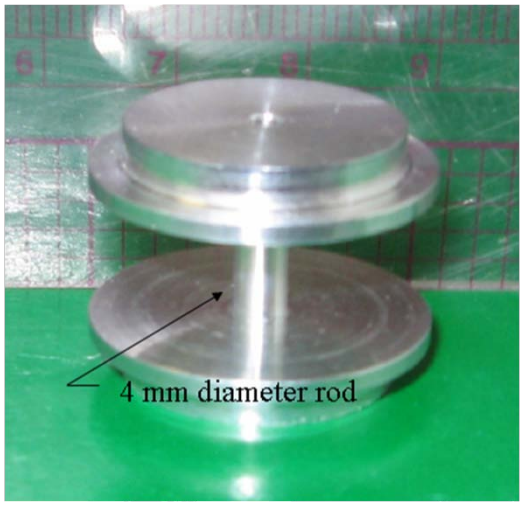

Figure 11. Photo. Solid rod for determining machine compliance correction.

The solid rod fixture shown in figure 11 was then attached to the disposable plate holders, and the compliance was determined by varying the angular motor displacement and measuring the torque generated in the same manner reported by Schroter et al. [2006]. Figure 12 is a plot of the torque versus the motor movement or twist. The data was generated by first inputting a fictitious gap (.001 mm in this case) and then performing a series of steps in strain starting off with the smallest value allowed and increasing in small increments to avoid reaching the maximum torque limit and damaging the torque transducer. Each strain step was applied for 100 seconds. The resulting torque and displacement for each step were averaged (note the very early times were ignored to avoid any ramp issues). The slope of the linear best fit line is the instrument compliance. This method was communicated to WRI by Hutcheson [2009].

The instrument compliance of WRI's ARES rheometer using the solid rod geometry was 0.02451 rad/Nm. A similar value of 0.02495 rad/Nm for WRI's ARES rheometer with 4-mm diameter aluminum plates was reported by Sui et al. [2010] using the solid rod fixture shown in figure 11.

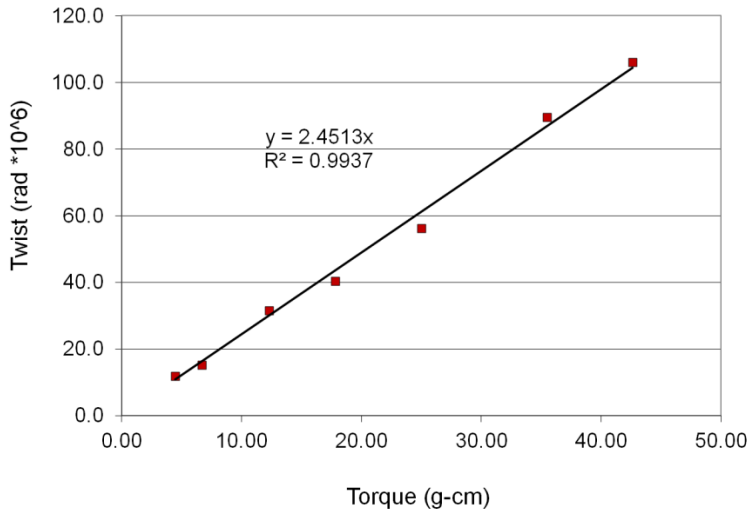

Figure 12. Graph. Measuring instrument compliance with a solid aluminum rod.

Instrument Compliance Measured with SuperGlue™

While using the solid rod fixture to measure instrument compliance we found it very difficult to mount the rod into the rheometer. The slightest misalignment would cause the rim of the rod to catch on the plate holder which could damage the normal force transducer and misalign the instrument.

A simpler alternative to the solid rod fixture was to use SuperGlue™ (cyanoacrylate) to chemically weld the plates together creating in effect a solid rod. After gluing the plates together the procedure to measure the instrument compliance is the same as outlined above for the solid rod. Details of the method can be found in the draft method in the Appendix under A2. Instrument Compliance Measurement and Calculation.

The instrument compliance for WRI's ARES with 4-mm diameter aluminum plates determined using SuperGlue™ was 0.02365 rad/Nm, which is comparable to the instrument compliance using the solid rod fixture (0.02451 rad/Nm) and the calculated instrument compliance using Schroter's reported ARES instrument compliance adjusted for 4-mm diameter aluminum plates (0.02265 rad/Nm).

While determining the instrument compliance using the SuperGlue™ method we tried several frequencies to evaluate the frequency dependence of the instrument compliance. It appeared that at least for the ARES and AR-G2 the instrument compliance was frequency dependent. Instrument compliance frequency dependency is considered in the next section.

Instrument Compliance Correction - Frequency Sweep Dependency

The rheometer torque transducer has a finite stiffness and the angular displacement is not zero. Similarly the rheometer test fixture itself deforms slightly due to the applied torque. Both

compliance contributions are important when the sample is stiff compared to the instrument. The test fixtures compliance is constant behaving in a purely elastic manner. However, the force rebalance transducer (FRT) has a response time controlled by the servo loop and therefore the compliance changes with frequency [Franck 2006].

Both the ARES and AR-G2 rheometers have FRT's. The frequency dependence of the instrument compliance for these two rheometers is tabulated in table 1. The instrument compliance of ARES shows very little frequency dependence which indicates the frequency dependence of instrument compliance for the ARES is relatively negligible. It appears the instrument compliance (0.02365 rad/Nm) determined using SuperGlue as shown in the previous section is a reasonable value to use for the real-time instrument compliance.

Table 1. Instrument compliance different frequencies for WRI's ARES and AR-G2 rheometers.

Rheometer	ω (rad/s)	Compliance (rad/N m)	Average (rad/N m)	Off [1] (%)
ARES	1	0.0238	0.02365	0.63
	10	0.0235		-0.63
ARG2	1	0.0222	0.0216	2.78
	5	0.0215		-0.46
	10	0.0211		-2.31

[1]Off with respect to average.

However, the AR-G2 instrument compliance appears more dependent on frequency and its dependence was re-measured at a wider range of frequencies (0.1 to 50 rad/s) as tabulated in table 2. Stress sweeps rather than strain sweeps were used. The results indicate the instrument compliance decreases with frequency. The AR-G2 instrument compliance values from table 2 are plotted in figure 13. The difference in instrument compliance between 0.1 and 50 rad/s is 12.8% and figure 13 suggests an exponential decay of compliance with frequency.

Table 2. Machine compliance at different frequency for the ARES and AR-G2 rheometers.

Rheometer	ω (rad/s)	Compliance (rad/N m)	Deviation (%)
ARES	1	0.0238	0.84*
	10	0.0236	
AR-G2	0.1	0.0226	12.8**
	0.5	0.0218	
	1	0.0214	
	5	0.0208	
	10	0.0206	
	50	0.0197	

* Percentage of difference of compliance at 10 rad/s with respect to that at 1 rad/s

** Percentage of difference of compliance at 50 rad/s with respect to that at 0.1 rad/s

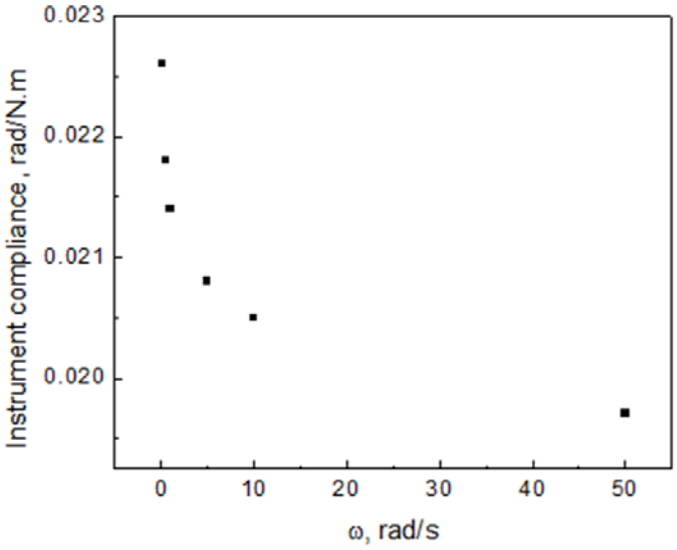

Figure 13. Graph. Instrument compliance of the AR-G2 rheometer as function of frequency.

The decrease in instrument compliance of the AR-G2 with frequency is caused by instrument inertia. The AR-G2 is a stress controlled rheometer consisting of a motor with a drive shaft and position sensor. It is also called a single head rheometer, in which the torque output of the motor includes the torque required to overcome instrument inertia as well as the torque for deforming the sample. At higher frequency, higher torque is required to overcome instrument inertia [Franck 2005], leading to a lower measured instrument compliance. Unlike the AR-G2, the ARES is a double head rheometer in which the motor deforms the sample and a transducer independently measures the torque. Therefore, the ARES is much less susceptible to inertia effects. Generally, inertia effects on the ARES are negligible for a test frequency below 100 rad/s [Franck 2005].

One solution to the frequency dependency of the AR-G2 instrument compliance is to consider modifying the instruments software algorithm to adjust the compliance correction for frequency using for example a power law.

Manually Correcting G'(ω) and G''(ω) for Instrument Compliance

Rides proposed a method to correct the dynamic moduli $G'(\omega)$ and $G''(\omega)$ due to instrument compliance in 1996. Schröter et al. [2006] and Franck [2006] have published similar methods. These methods can be used when real-time online instrument compliance correction by the rheometer software is unavailable, or when the user wants to check the software calculation.

TA Instrument software from version 7.00 allows input of the instrument compliance and corrects the dynamic moduli Franck [2006]. Sui et al. [2010] were the first to apply instrument compliance correction to asphalt binder low temperature oscillatory shear dynamic moduli (~ 5°C to -40°C).

To check and compare the ARES software (Version 7.2.0.4) dynamic moduli instrument compliance correction to manual correction, the manual correction was performed using the methods published by Franck [2006] and Rides [1996]. The corrections were performed on a -24°C frequency sweep obtained using WRI's ARES rheometer. Two frequency sweeps were investigated: one with the instrument compliance set to zero and the other with the instrument compliance set to the measured instrument compliance for the ARES with 4-mm diameter parallel aluminum plate geometry.

Figure 14 compares the uncorrected and corrected dynamic moduli using the Franck and Rides methods and the ARES software output. The Franck and Rides methods result in very similar corrected dynamic moduli and the Rides and Franck manually corrected dynamic moduli methods compare favorably to the ARES software corrected dynamic moduli, but are not exactly the same. Keep in mind that there are two separate frequency sweeps. That is, we are taking the uncorrected data where we set the instrument compliance to zero and correcting it and comparing it to a different run where we set the instrument compliance to the proper value.

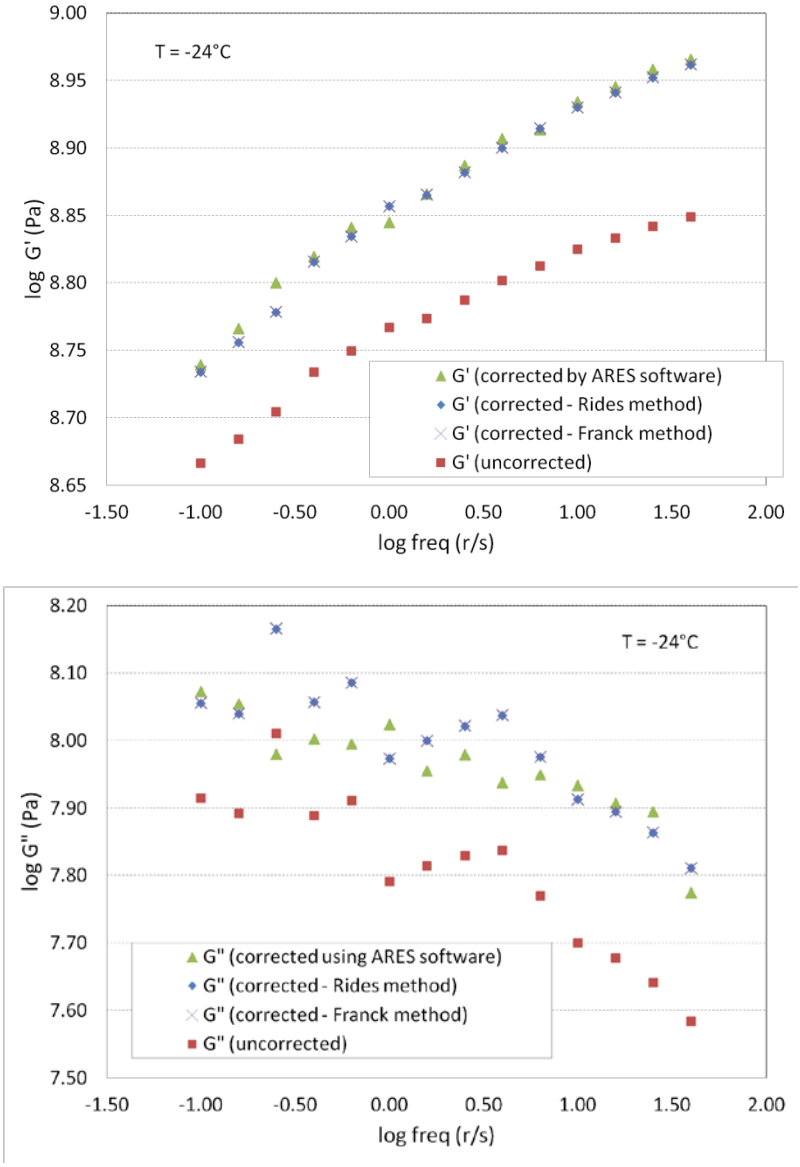

Figure 14. Graph. Instrument compliance correction - comparison of uncorrected and corrected dynamic moduli' frequency sweeps. Instrument compliance was corrected using three methods: (1) ARES software (ver. 7.2.0.4), (2) Rides [1996], and (3) Franck [2006].

The following is a mathematical method for correcting errors in the dynamic moduli $G'(\omega)$ and $G''(\omega)$ due to instrument compliance and can be used when real-time online instrument compliance correction by the rheometer software is unavailable or to check the instrument correction. The method is also provided in the Appendix (A1. Instrument Compliance Correction).

When the rheological measurements are on stiff samples or at low temperatures, the actual measured angular displacement (θ_m) includes the sample angular displacement (θ_s) and the machine or tool angular displacement (θ_t).

$$\theta_m = \theta_s + \theta_t$$

Figure 15. Equation. Angular displacement.

The torsional stiffness K is related to the angular displacement θ and the torque M as follows:

$$K = \frac{M}{\theta}$$

Figure 16. Equation. Torsional stiffness.

Under the applied torque M,

$$\frac{1}{K_m} = \frac{1}{K_s} + \frac{1}{K_t}$$

Figure 17. Equation. Measured compliance.

Where K_m is the measured stiffness, K_s is the sample stiffness, and K_t represents the machine or fixture tool stiffness.

By rearranging figure 17, the sample stiffness can be obtained as

$$K_s = \frac{K_m K_t}{K_t - K_m}$$

Figure 18. Equation. Sample torsional stiffness.

To convert the torsional stiffness (K) into shear modulus (G), the geometry constant or the geometry conversion factor (k_g) needs to be introduced.

$$K = {}^{G}/_{k_g}$$

Figure 19. Equation. Torsional stiffness.

For example, for the parallel plate fixture geometry with plate radius R and gap between plates of h,

$$k_g = \frac{2h}{\pi R^4}$$

Figure 20. Equation. Geometry conversion factor.

Due to the viscoelastic characteristics of samples, both the measured and sample stiffness and moduli are in the complex form, while the fixture tool only has the real part value by assuming the tool material is purely elastic.

So the machine or tool compliance (J_{tool}) can be simply expressed as

$$J_{tool} = \frac{1}{K_t}$$

Figure 21. Equation. Machine compliance.

Substituting figures 19 and 21 into figure 18 gives

$$G_s^* = \frac{G_m^*}{1 - \frac{J_{tool}}{k_g} G_m^*}$$

Figure 22. Equation. Sample complex modulus.

Where G_s^* and G_m^* are the sample complex modulus and the measured complex modulus respectively. For the parallel plate geometry, the sample complex shear modulus is

$$G_s^* = \frac{G_m^*}{1 - J_{tool}\, G_m^* \frac{\pi R^4}{2h}}$$

Figure 23. Equation. Complex modulus with parallel plate geometry.

Figure 22 can be rewritten in the form of storage and loss moduli as

$$G_s^{'} + iG_s^{"} = \frac{G_m^{'} + iG_m^{"}}{1 - \frac{J_{tool}}{k_g}(G_m^{'} + iG_m^{"})}$$

Figure 24. Equation. Storage and loss moduli with parallel plate geometry.

By rearranging figure 24, the storage ($G_s^{'}$), loss ($G_s^{"}$) moduli and phase angle (δ_s) of the sample can be calculated as

$$G_s^{'} = \frac{G_m^{'}\left(1 - \frac{J_{tool}}{k_g} G_m^{'}\right) - \frac{J_{tool}}{k_g} G_m^{"\,2}}{\left(1 - \frac{J_{tool}}{k_g} G_m^{'}\right)^2 + \left(\frac{J_{tool}}{k_g} G_m^{"}\right)^2}$$

Figure 25. Equation. Storage modulus.

$$G_s^{"} = \frac{G_m^{"}}{\left(1 - \frac{J_{tool}}{k_g} G_m^{'}\right)^2 + \left(\frac{J_{tool}}{k_g} G_m^{"}\right)^2}$$

Figure 26. Equation. Loss modulus.

$$tan(\delta_s) = \frac{G_m^{"}}{G_m^{'}\left(1 - \frac{J_{tool}}{k_g} G_m^{'}\right) - \frac{J_{tool}}{k_g} G_m^{"\,2}}$$

Figure 27. Equation. Phase angle.

Comparing Machine Compliance Corrected 4-mm DSR Data and Intermediate and High Temperature 8 and 25 mm Parallel Plate Data

Figure 28 compares the *G*(ω)* master curve for a PAV aged asphalt combining the data collected using 4-mm DSR at temperatures ranging from -30 to 30°C and the *G*(ω)* master curve of the same asphalt using 8 mm and 25 mm parallel plates at intermediate and high temperatures ranging from 0 to 80°C. The machine compliance corrections for 4-mm parallel plate data were done automatically by inputting a compliance value to the system software. The comparison of the two master curves in figure 28 indicates: (1) the data collected on different size platens are consistent with each other; and (2) DSR reliably reproduces data using different size plates after machine compliance corrections are applied.

Consistency between Data Collected with 4-mm Parallel Plates on Both ARES and AR-G2 after Machine Compliance Correction

Dynamic frequency sweep tests on a PAV aged binder at temperatures ranging from -30 to 30°C were conducted on both WRI's ARES and ARG2 rheometers with real time machine compliance corrections. The resulting master curves of *G** are shown in figure 29. It appears that both rheometers generated similar data after machine compliance correction. This indicates the validity of 4-mm DSR technique.

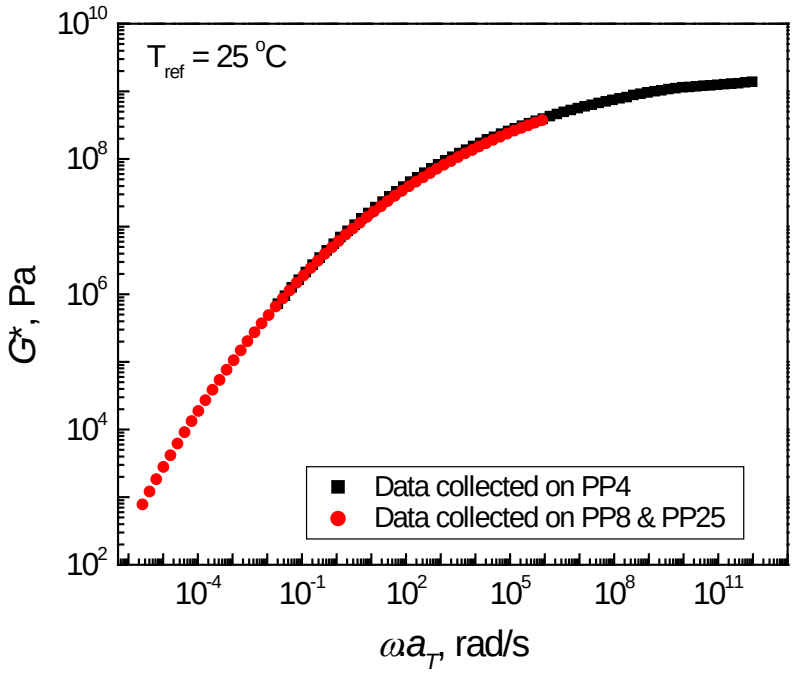

Figure 28. Graph. Master curves of *G** combining data collected on DSR with 4, 8 and 25 mm parallel plates for a PAV aged asphalt (PP4 = parallel plate geometry, 4 mm diameter plates; PP8 = parallel plate geometry, 8 mm diameter plates).

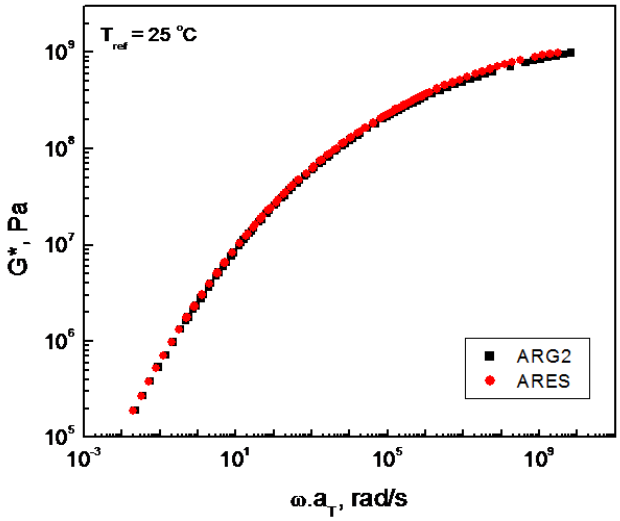

Figure 29. Graph. Master curves of *G** of a PAV aged asphalt binder based on 4-mm DSR using both ARES and ARG2 instruments after machine compliance correction.

Angular Velocity and Plate Slippage and/or Sample Breakage during Oscillatory Shear at Low Temperature

It has been observed on occasion that one or more of the frequency sweeps at very low temperature (typically -30°C or lower) appears erroneous. That is, when plotted on a black space plot the frequency sweep clearly differs from the trend established by the warmer frequency sweeps. The reason is attributed to plate slippage or specimen micro-fracture, or a complete fracture of the specimen, or some combination of the three. Specimen stiffness plays a role … highly oxidized binder tends to lose adhesion or fracture more often than unaged binder.

In order to address the slippage occurring during oscillatory shear at very low temperature, consideration is being given to modifying the surface of the parallel plates to increase adhesion. Several modifications are under consideration: cross hatching, mild sand blasting, adding micro-cleats, etc. However, there may be several simpler alternatives to address the problem.

Initially, frequency sweeps during 4-mm plate DSR were performed from 0.1 to 100 rad/s at low and intermediate temperatures. However, it appears that at temperatures below approximately 0°C the frequency sweep range should be modified to 0.1 to a maximum 50 rad/s or possibly less. The actual temperature where the revised range is required varies depending on the brittleness/ductility of the sample being tested.

To explore the effect of limiting the plate velocity to 50 rad/s, a stiff asphalt from the WRI/FHWA Arizona comparative test site was tested with both ranges. Standard 4-mm plate DSR frequency sweeps were performed at 30, 15, 0, -15, -30, and -40°C on two specimens of the Arizona asphalt where the only difference was the range of the frequency sweeps: 0.1 to 50 rad/s and 0.1 to 100 rad/s.

As shown in figure 30, it appears that limiting the plate velocity to 50 rad/s can make a significant difference in terms of improving adhesion and/or fracture. Both samples appeared to fail at -40°C in terms of adhesion and/or fracture.

The -40°C freq sweep for the 50 rad/s test was stopped after a few early frequencies and is not shown on the plot in figure 30. The -40°C freq sweep for the 100 rad/s was continued and the loss of adhesion is apparent. However, the -30°C frequency sweep for 50 rad/s sweep looks correct and there was no apparent plate slippage or fracture, while the 100 rad/s clearly lost some adhesion or was partially fractured.

Another simple method to resolve the plate adhesion issue could be to simply increase the temperature during the sample loading process onto the plates. Currently the 4-mm DSR method requires 5 minutes at 60°C.

Scoring the plates, along with reducing the upper limit of the frequency sweeps and increasing the temperature during loading will be investigated during ruggedness testing.

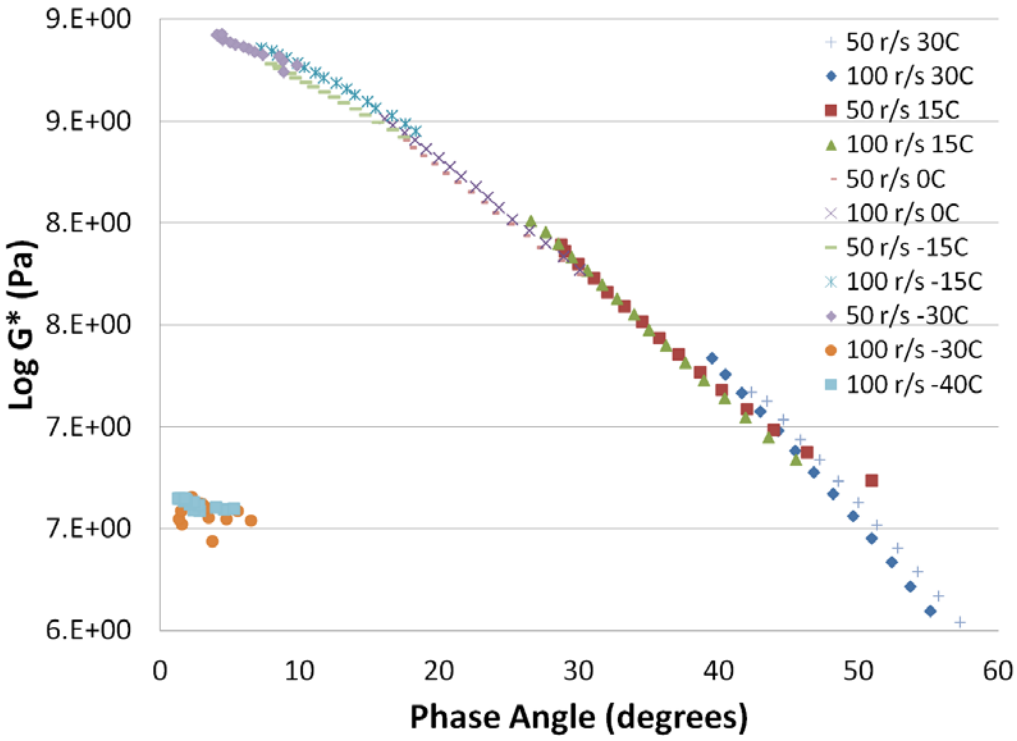

Figure 30. Graph. Comparison 50 and 100 rad/s max. frequency sweeps.

A Low-temperature Performance Grading Method Using 4-mm DSR

Low-temperature rheological parameters such as BBR m-value and creep stiffness S(t) can be estimated through a correlation with 4-mm DSR developed by Sui et al. [2011]. Figure 31 illustrates the Sui et al. method. The slope and magnitude of the shear stress relaxation modulus *G(t)* master curve at 2 hours and at the true low PG grading temperature are correlated with the corresponding *S*(*t*) and m-values at 60 seconds and 10°C above the true low PG grading temperature from BBR measurements.

Figures 32 and 33 show the Sui et al. [2011] correlation developed between BBR creep stiffness and DSR shear stress relaxation data allowing estimation of BBR m-value and S(t) from 4-mm DSR. A strong linear correlation between BBR and DSR data was observed based on eleven asphalt binders.

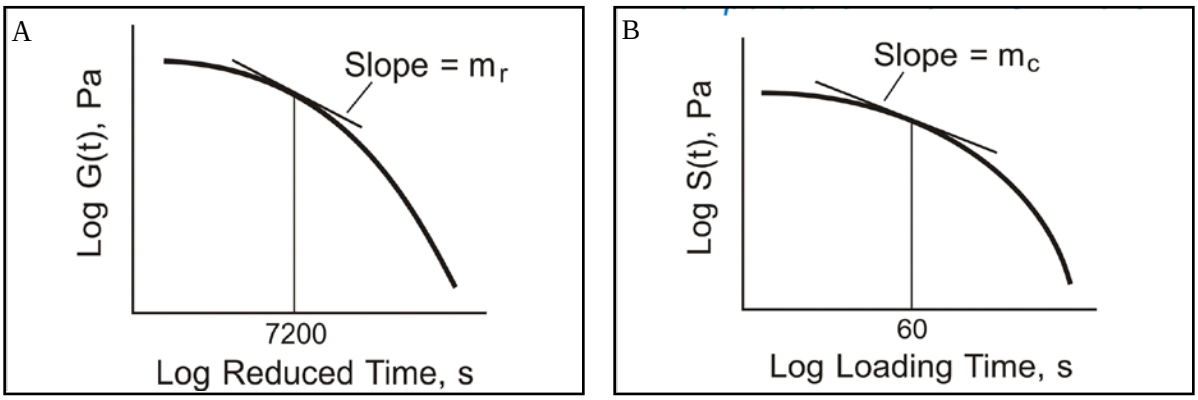

Figure 31. Graph. A: 4-mm DSR - relaxation modulus G(t) and the slope at 2 hours. Reference temperature is equal to the low PG temperature. B: BBR - creep stiffness and m-value at 60 seconds. Reference temperature is equal to the low PG temperature plus 10°C.

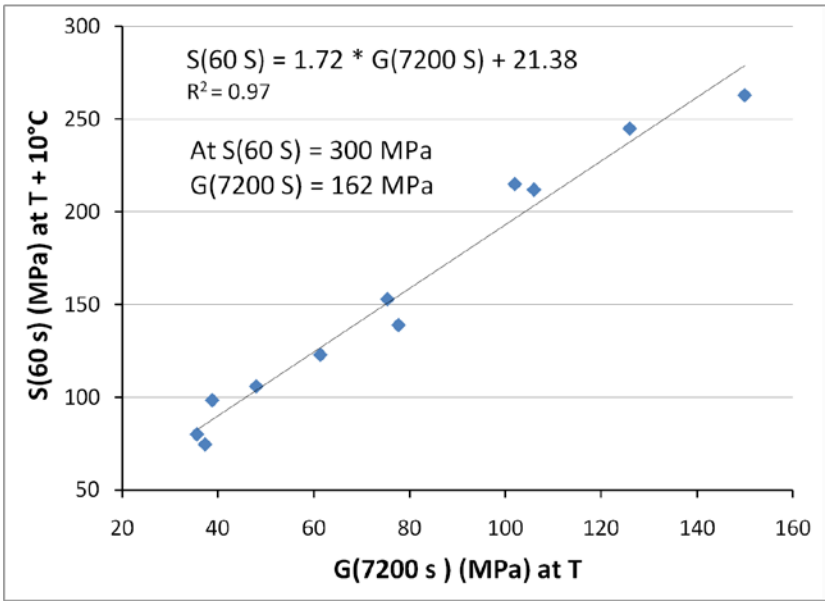

Figure 32. Graph. Correlation between BBR S(60s) and 4-mm DSR G(7200 s) [Sui et al. 2011].

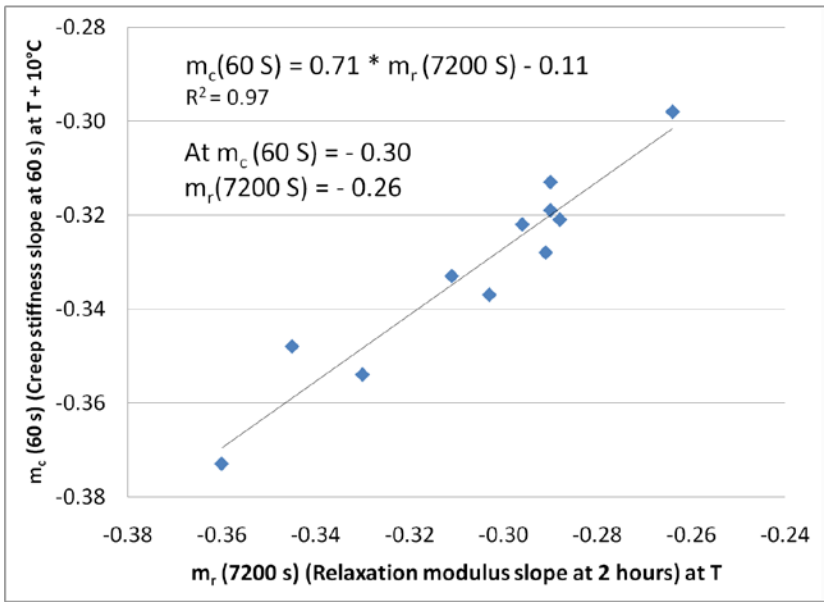

Figure 33. Graph. Correlation between BBR m_c(60s) and 4-mm DSR mr(7200 s) [Sui et al. 2011].

The Sui et al. [2011] method relating BBR and 4-mm DSR has been recently modified by measuring the *G(t)* slope and magnitude at 60 seconds and 10°C higher than the PG grading temperature. The reasons for the modifications are that they significantly reduce test time, and the test temperature is easier to achieve, and hence, reduces potential error. This has been adopted for the method in the Appendix.

The original data in the Sui et al. [2011] study were revisited and a new correlation was developed between BBR and 4-mm DSR by comparing the *G(t)* slope and magnitude at 60 seconds and 10°C higher than the PG temperature, rather than at 7200 seconds and at the PG temperature. Figures 34 and 35 show the correlations using this new approach. Table 3 compares this approach to the original Sui et al. correlation [2011].

The Sui et al. [2011] and the modified approach discussed above are relatively similar and should be considered tentative pending ruggedness testing to evaluate the effect of the cooling rate and time at temperature during DSR testing. Both effects are related to physical hardening.

Table 3. Comparison of original Sui et al. [2011] approach and revised approach at T + 10°C.

Correlation approach	S(60 s) = 300 psi	Correlation approach	m_c = -.30
G(7200 s) (MPa) at PG temp	162	m_r(7200 s)	-0.26
G(60 s) (MPa) at PG temp +10°C	143	m_r (60 s)	-0.28

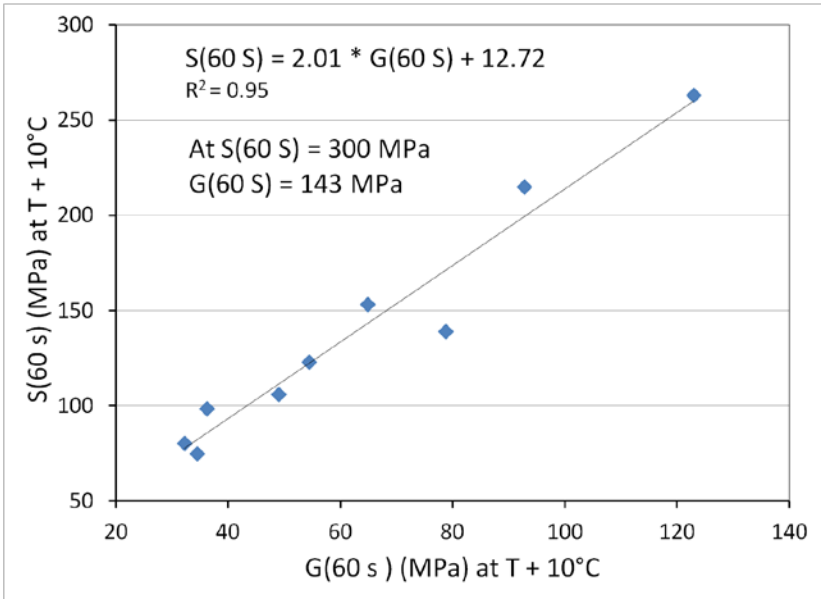

Figure 34. Graph. Correlation between BBR S(60s) and 4-mm DSR G(60 s).

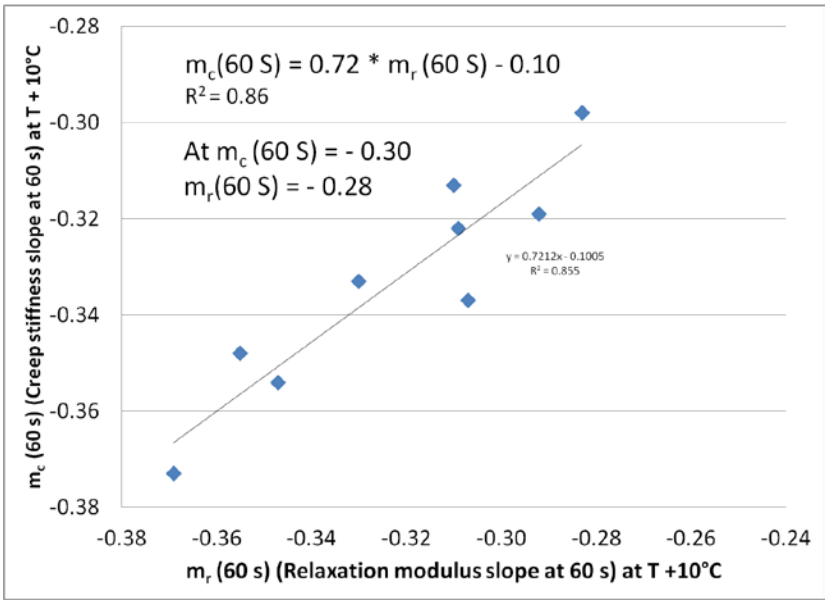

Figure 35. Graph. Correlation between BBR m_c(60s) and 4-mm DSR m_r(60 s).

How to Determine m_r and G(t)

As mentioned above the 60 second approach at a 10°C warmer temperature to estimate BBR m-value and creep stiffness based on the slope m_r(60 s) and magnitude of the relaxation modulus *G*(60 s) has been adopted for the method in the Appendix.

A series of steps are involved when calculating m_r (60 s) and *G(t)* from dynamic oscillatory shear data (two frequency sweeps in this case) at 60 seconds and a reference temperature of PG+10°C. The first step is to generate a *G'(ω)* master curve at a reference temperature of PG+10°C using PG+10°C and PG+20°C frequency sweeps.

A typical representation of test data is shown in figure 36.

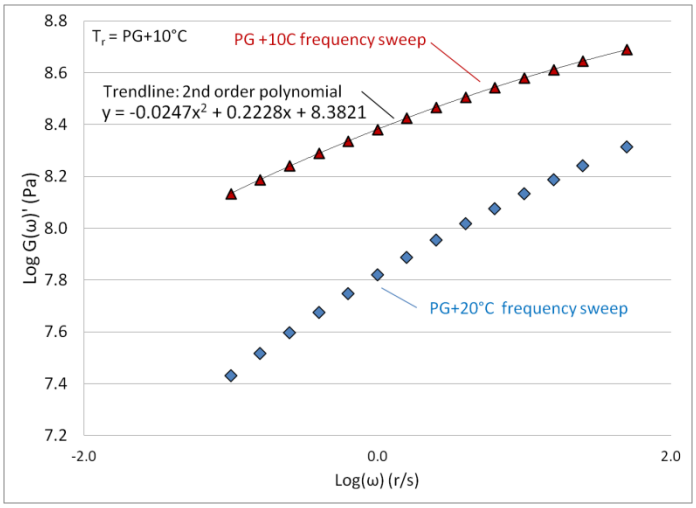

Figure 36. Graph. PG+10°C and PG+20°C frequency sweeps.

The next step involves using Excel™ solver to determine the horizontal shift factor (a_T) to translate the PG+20°C frequency sweep along the abscissa so that it overlaps the PG +10°C frequency sweep. The horizontal translation is accomplished by multiplying the PG+20°C frequencies by a_T and plotting the storage modulus as a function of the multiplied frequencies. The basis for the shift factor is known as time-temperature superposition (TTS). Figure 37 demonstrates the calculation of the shift factor. To avoid error from extrapolation of the 2nd order polynomial, only *G'(ω)* data that approximately overlap are used to estimate a_T. The resultant *G'(ω)* master curve is shown in figure 38.

Least squre difference (LSD) (log G' freq. sweep — calculated log G' based on 2nd order polynomial)^2

Solver—changing cell

ω (r/s)	log ω (r/s)	G' from PG+20°C ω sweep (Pa)	log G' (Pa)	Shift factor = 0.0103	aT * ω (r/s)	log (aT * ω) (r/s)	log G' (2nd order polynomial) from figure 1) (Pa)	LSD
3.98	0.60	1.04E+08	8.02	Sum LSD = 7.93E-06	4.08E-02	-1.39	8.02	3.26E-06
6.31	0.80	1.19E+08	8.08		6.47E-02	-1.19	8.08	1.72E-06
10.00	1.00	1.36E+08	8.13		1.03E-01	-0.99	8.13	3.60E-07
15.85	1.20	1.54E+08	8.19		1.63E-01	-0.79	8.19	1.91E-07
25.12	1.40	1.74E+08	8.24		2.58E-01	-0.59	8.24	1.58E-06
39.81	1.60	1.95E+08	8.29		4.08E-01	-0.39	8.29	2.19E-07
50.00	1.70	2.06E+08	8.31		5.13E-01	-0.29	8.31	6.03E-07

Solver target cell

Figure 37. Illustration. Estimating the horizontal shift factor a_T using Excel™ Solver.

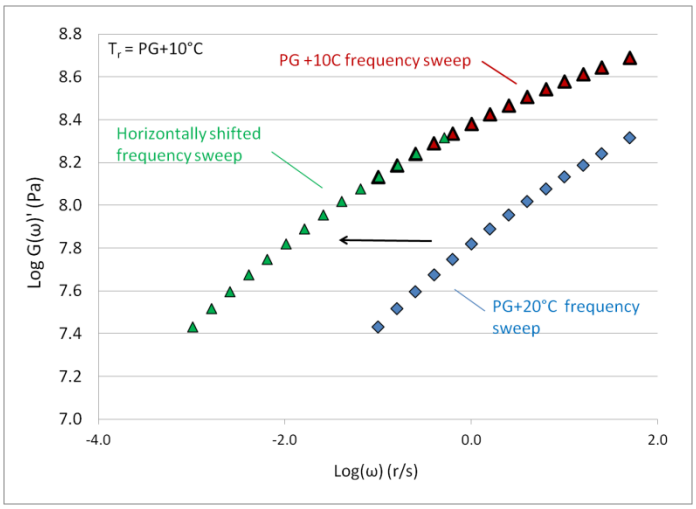

Figure 38. Graph. *G'* Master curve at a reference temperature PG+10°C.

The relaxation modulus *G(t)* is then determined thru interconversion of the storage modulus *G'(ω)* by the approximate expression developed by Christensen [1982].

$$G(t) \approx G'(\omega)|_{\omega=2/\pi t}$$

Figure 39. Equation. Shear relaxation modulus.

Figure 40 displays the relaxation modulus determined using figure 39. The relaxation modulus is fit with a 2nd order polynomial using the time points that bracket 60 seconds (0.78 to 2.78 in log scale) to generate the polynomial. The slope of the relaxation modus at 60 seconds is determined by taking the first derivative of the 2nd order polynomial. Additional details on the method to determine mr(60 s) and G(60 s) can be found in the Appendix, A4.

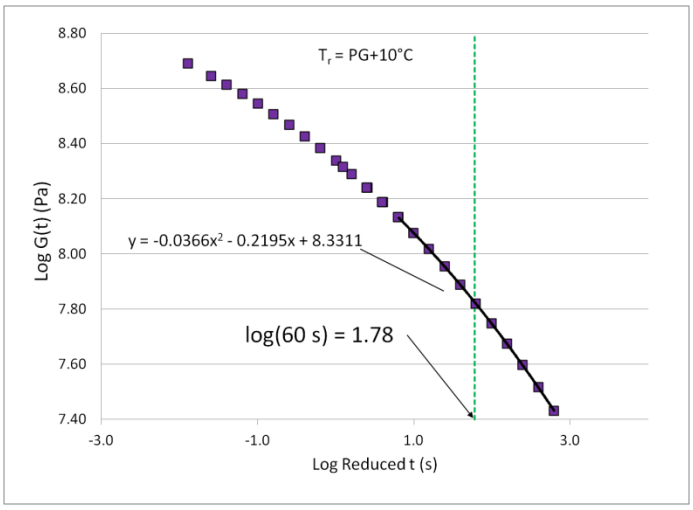

Figure 40. Graph. Relaxation modulus master curve to determine mr(60 s) and G(60s).

Physical Hardening and 4-mm DSR

Physical Hardening and Strain Level

Few studies have been reported on asphalt binder physical hardening effects during a DSR test with parallel plate geometry at low temperature. Which is not surprising since an instrument compliance correction method was only recently developed, and DSR data obtained with the parallel plate geometry were unreliable when the temperature approached the glass transition region without instrument compliance correction.

The results of an initial physical hardening experiment performed in the early stages of the 4-mm DSR development are shown in figure 41. The sample, after initial annealing and then cooling to -20°C was kept between the plates and frequency sweeps were performed at different physical aging times. Figure 41 shows that a large increase in complex shear modulus was observed after about two hours, but little increase was observed after that.

However, BBR beams which are unconstrained, continue to physically harden for weeks at low temperature [Bahia and Anderson 1993]. It appears, at least in this experiment, that physical hardening in a DSR dramatically slows down or ceases after several hours. It is speculated the lateral constraint of the plates played a significant role in slowing the physical hardening.

In terms of strain level, two strain levels were evaluated: 0.005% and 0.01% at time zero. Both strain levels were well within the linear viscoelastic range, however, it was hypothesized that the higher strain level, even if it was still within the linear range, might disrupt the micro-structuring associated with physical hardening to a greater extent than the lower strain level. The time zero results, as shown in figure 41 suggest the increased strain level did not have a significant effect on G^*.

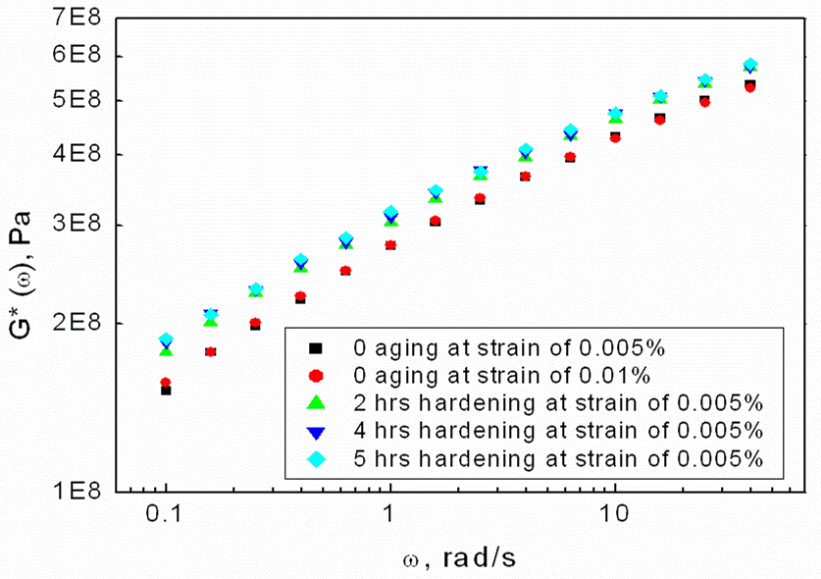

Figure 41. Graph. Physical hardening. RTFO/PAV aged polymer modified asphalt, T_{ref} = -20˚C. Note: time zero was after 20 minutes at -20°C.

Physical Hardening and Thermal History

Tabatabaee et al. [2012] have recently proposed that laboratory observed physical hardening can be modeled as a function of isothermal time by a modified mechanical creep model. The developed creep model predicts physical hardening as a function of glass transition, conditioning time, and temperature. The model can be used to predict changes in BBR parameters (i.e., S(60 s) and m(60 s)) after various isothermal conditioning times. Tabatabaee et al. also provide an excellent summary of the literature on physical hardening as it relates to asphalt binder and mixes.

Tabatabaee et al. point out that incorporation of physical hardening into thermal stress/strain calculations is a critical need in the current thermal cracking analysis framework. WRI is currently evaluating the proposed creep model and considering applying a similar approach to the observed physical hardening during 4-mm DSR. However, rather than creep, we would develop the model in terms of relaxation.

In the Tabatabaee et al. creep model the glass transition is an important parameter, perhaps the critical parameter, and Tabatabaee et al. state “no model can accurately describe it [physical hardening] without taking the glass transition into account.” Tabatabaee et al. used a dilatometric system to measure the glass transition temperature of the asphalt binders. For unmodified and modified asphalts, a plot of the loss modulus (*G''*) from 4-mm DSR versus temperature results in a curve which usually exhibits a peak value. The temperature at this peak value can be interpreted as the glass transition temperature (Tg). The G" peak value is dependent on the cooling rate and the test frequency [Pink et al.1980; Anderson et al. 1999; Reinke and Engber 2002; Kriz 2009].

A plot of *G″* using bending beam rheometer creep compliance data is possible through interconversion, however using 4-mm DSR data is simpler and more accurate since *G″* is measured directly during 4-mm DSR testing.

Incorporation of physical hardening into thermal stress/strain calculations is an important goal; however, the short term goal for 4-mm DSR is to develop AASHTO and ASTM methods and associated specifications that allow 4-mm DSR as an alternative to the BBR. In other words, the short term goal is to provide a 4-mm DSR method that will result in similar low temperature performance grading compared to the BBR. That's because refineries that supply asphalt have become quite adept in blending and modifying asphalt to meet the low temperature performance grade requirements using BBR. If a specifying agency wants to adopt 4-mm DSR rather than BBR, they want to be confident, at least initially, that the current blending and modifying strategies that refineries have developed are still valid. To put it more bluntly, it would not be desirable to have refineries calling specifying agencies that with the new 4-mm DSR method a significant portion of their blends and modified asphalt don't meet the low temperature specification requirements, but the previous year using the BBR method all of their blends easily met the low temperature specification requirements.

With the short term goal of developing an alternative to BBR in mind, several 4-mm DSR tests were performed on the SHRP core asphalt AAM-1 that had been oxidatively aged in accordance with standard AASHTO RTFO and PAV methods. AAM-1 was derived from a West Texas Intermediate crude oil and is relatively high in wax content compared to the other SHRP core asphalts. Research on asphalt and physical hardening has demonstrated that at low temperature the crystallized wax fraction appears to play a significant role in physical hardening occurring with time [Planche et al. 1998; Anderson and Marasteanu 1999; Bahia et al. 2000].

Sui et al. [2011] have demonstrated, using eleven asphalts, that BBR m-value and creep stiffness S (t) can be estimated through a correlation with 4-mm DSR. In the present study, AAM-1 is used as a worst case example. If AAM-1 when tested using 4-mm DSR provides comparable BBR m-value and creep stiffness (S(t)) then the current 4-mm DSR methodology can be considered as essentially meeting the initial goal of representing an alternative to BBR.

In the Sui et al. method, the slope and magnitude of the shear stress relaxation modulus *G(t)* master curve at 2 hours and at the true low PG grading temperature are correlated with the corresponding *S*(*t*) and m-values at 60 seconds and 10°C above the true low PG grading temperature. The Sui et al. method was modified by measuring *G(t)* slope and magnitude at 60 seconds and 10°C higher that the PG grading temperature. See the section in this report titled *A Low-temperature Performance Grading Method Using 4-mm DSR* for further discussion and detail.

DSR measurements were performed employing two methods: (1) The Method in the Appendix and (2) a method we currently use to develop asphalt binder master curves of the dynamic moduli at low, intermediate and high temperature which involves performing frequency sweeps at 15°C intervals over a temperature range of -30 to 30°C employing 4-mm plate geometry, and frequency sweeps at 50°C and 70°C employing 25 mm plate geometry. An angular frequency range of 0.1 to 50 rad/s was used at all temperatures.

The thermal regimes between the two methods are different. In both methods the sample is loaded into the rheometer employing the same times and temperatures, however, with method (1) after loading, the temperature is immediately changed to the low PG temperature plus 20°C and allowed to equilibrate at that temperature for 20 minutes, then a stress sweep and frequency sweep are performed which require approximately 30 minutes. The temperature is then changed to the PG temperature plus 10°C and the same times for equilibration and testing are required. That's it for method (1), only two frequency sweeps are required.

For method (2), the thermal history is shown in table 4.

Table 4. Method (2) thermal regime.

Time (minutes)	Temperature (°C)	Process
20	30	Temperature stabilization
30	30	Stress and frequency sweep
20	15	Temperature stabilization
30	15	Stress and frequency sweep
20	0	Temperature stabilization
30	0	Stress and frequency sweep
20	-15	Temperature stabilization
30	-15	Stress and frequency sweep
20	-30	Temperature stabilization
30	-30	Stress and frequency sweep

Figure 42 compares the AAM-1 relaxation modulus master curves for both methods. The two master curves are very similar suggesting that the different thermal regimes did not cause a significant difference in physical hardening.

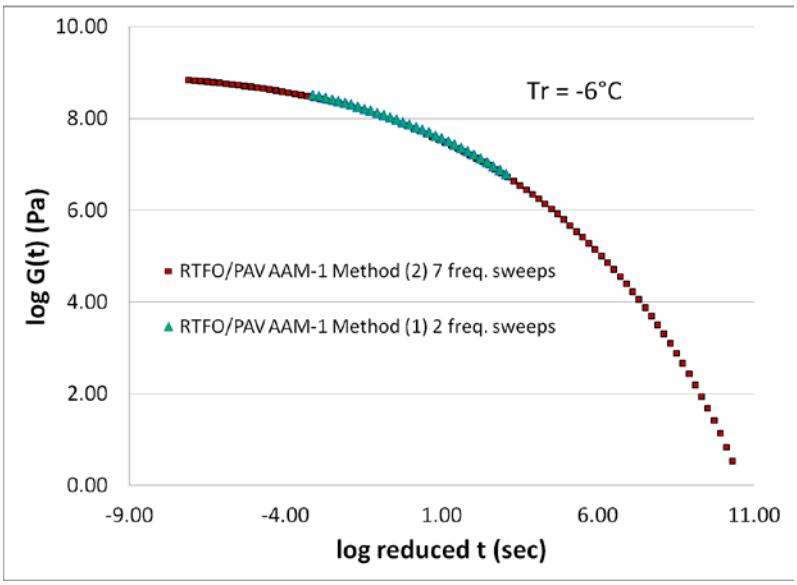

Figure 42. Graph. Relaxation modulus: Method (1) and (2) compared.

The BBR m_c(60s) and S(60s) at the PG +10°C temperature (-6°C in this case) are -0.35 and 80 MPa, respectively [average of several reported values]. Using the DSR data from Method (1) the calculated m_c(60s) and S(60s) are -0.36 and 53 MPa , respectively. The reported BBR and calculated 4-mm DSR values are quite close. The m-values are plotted in figure 43 along with the original data used to develop the correlation between BBR and 4-mm DSR. In addition, as noted in figure 43, MN1-4 was also derived from West Texas Intermediate and is known to contain significant wax and it too plots rather well on the calibration curve. Creep stiffness values are plotted in figure 44 and as with m-value, AAM-1 S(60s) plots reasonably well to the calibration curve.

It appears that 4-mm DSR, performed in accordance with the method in the Appendix, provides m-value and creep stiffness values that are comparable to standard BBR, even for asphalts with considerable crystalline fraction such as AAM-1.

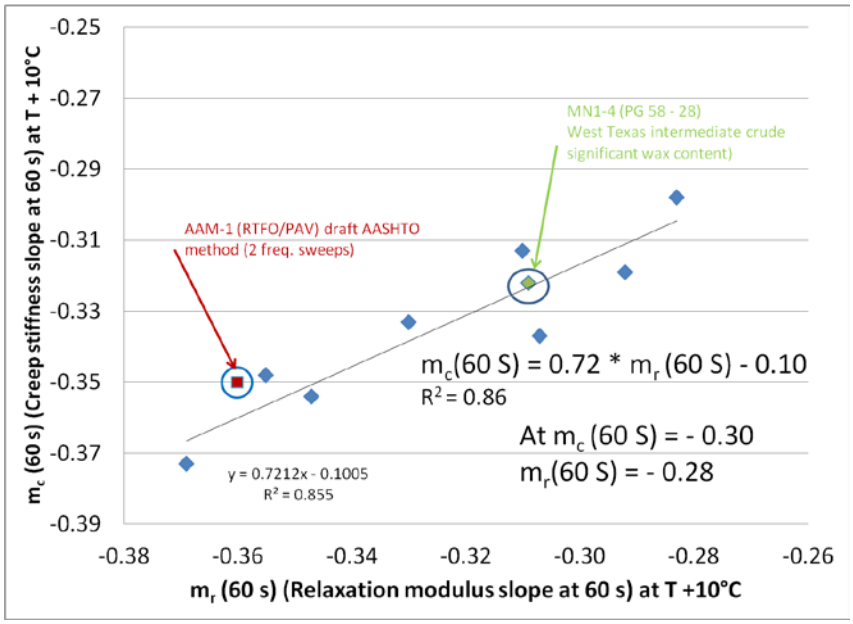

Figure 43. Graph. AAM-1 (RTFO/PAV) 4-mm DSR m-value result compared to calibration data developed from Sui et al. [2010].

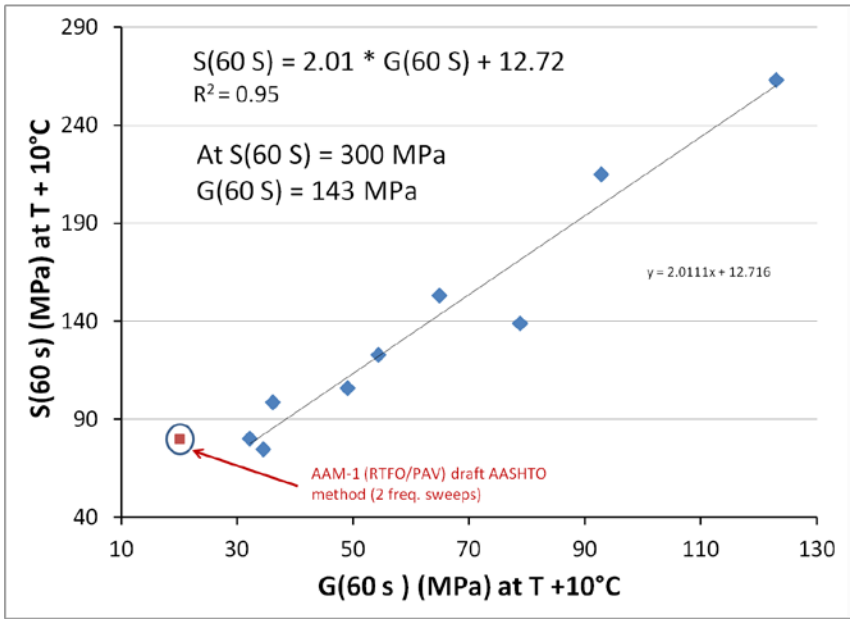

Figure 44. Graph. AAM-1 (RTFO/PAV) 4-mm DSR S(60s) result compared to calibration data developed from Sui et al. [2010].

Time - Physical Aging Time Superposition

It is almost always impractical in terms of instrument capability and laboratory time to evaluate material performance under the actual temperature and time conditions the material will see in the field. Fortunately, however, the method of time (or frequency) temperature superposition (TTS), overcomes the difficulty of extrapolating limited laboratory tests at shorter times to longer term, more real-world, conditions.

The basic assumption underlying TTS is that in a series of relaxation (or retardation) mechanisms a change of temperature multiples all relaxation (or retardation) times by the same factor. That is, a change in temperature from T_o to T results in a change in the relaxation (or retardation) time resulting in a temperature shift factor

$$a_T = \tau_{To}/\tau_T$$

Figure 45. Equation. Temperature shift factor.

where τ_{T0} represents the relaxation times at temperature T_o and τ_T represents the relaxation times at an increased or decreased temperature T.

Correspondingly, in a solution of a viscoelastic component of an ordinary viscous liquid a change in concentration multiplies all relaxation or retardation time by the same factor and the magnitude of each contribution to rigidity is proportional to the concentration (C) of the viscoelastic component [Ferry 1961]. As with TTS, a change in concentration from C_o to C will affect the characteristic relaxation time leading to a concentration shift factor [Shi 2004].

$$a_C = \tau_{Co}/\tau_C$$

Figure 46. Equation. Concentration shift factor.

where τ_{C0} represents the relaxation times at a concentration C_o and τ_C represents the relaxation times at an increased or decreased concentration C.

Marasteanu and Anderson [1996] suggested a similar relationship where a change in physical hardening multiplies all relaxation or retardation times by the same factor and the magnitude of each contribution to rigidity is proportional to the physical aging time. In actual practice, Marasteanu and Anderson chose to modify the standard Williams-Landel-Ferry (WLF) equation by adding an additional parameter to account for non-equilibrium conditions. Bahia and Anderson [1993] concluded similarly that the physical hardening of asphalt cements and associated shifting based on physical aging time can be directly related to a temperature based shift.

To evaluate time-physical aging time superposition and the evolution of asphalt binder stiffness towards equilibrium after quenching a simple experiment was performed on an unmodified PG 58-28 RTFO and PAV aged asphalt. After loading the sample onto 4-mm plates and stabilizing the temperature at 30°C, the sample was then quenched to a temperature of -20°C at an approximate cooling rate of 15°C/minute. A 20 minute stabilization time was allowed and then

the first of several dynamic shear frequency sweeps (0.1 to 50 rad/s) were performed. The frequency sweeps were performed over a period of about 6 hours. A stress sweep was performed prior to each frequency sweep to insure the stress test level was in the linear viscoelastic range. The experiment was performed on a Kinexus stress control rheometer with 4-mm parallel plate geometry and a temperature control system consisting of Peltier cooling coupled with a chiller allowing testing to -40°C. The normal force on the sample during testing fluctuated, but did not exceed 0.05 N.

When an asphalt at roughly room temperature is quenched to below the glass transition temperature the material is out of equilibrium and the thermodynamic state of the material evolves towards equilibrium. This evolution is shown in figure 47. *G** master curves prepared from frequency sweeps captured near or below the glass transition temperature potentially suffer significant error from this structural recovery process.

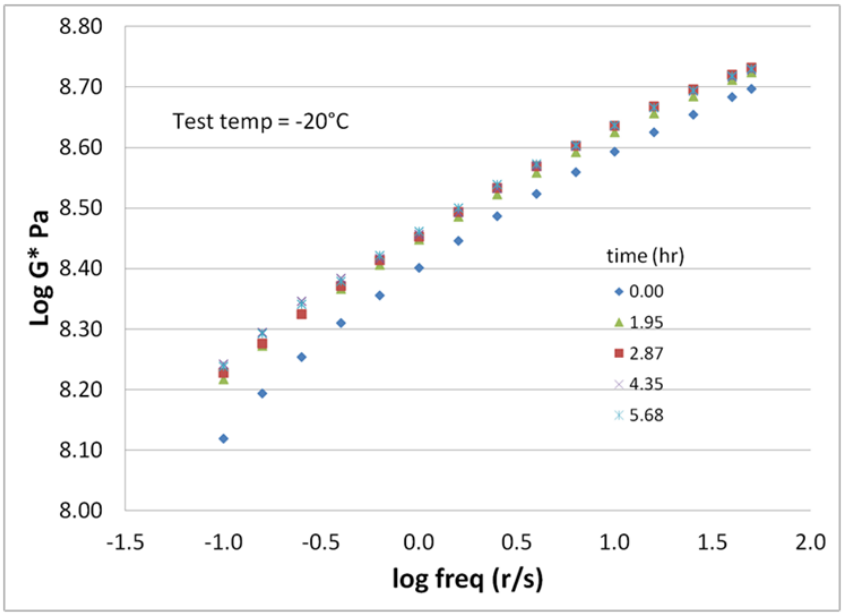

Figure 47. Graph. 4-mm plate DSR - frequency sweeps at different physical aging times, for an RTFO/PAV aged asphalt (PG 58-28). Time zero was after 20 minutes at -20°C.

In figure 48, the frequency sweeps shown in figure 47 were shifted to a zero reference physical aging time using polynomial pair-wise shifting in a manner similar to the method programmed in the early 1990's by Gordon and Shaw [1994]. A vertical shift did not appear necessary suggesting that the physical aging shift is in a sense thermorheologically simple and is similar to time temperature superposition.

Figure 49 is a plot of the log of the physical aging time shift factor ($a_{pt)}$ versus physical aging time derived from figure 47. It allows *G** master curve development at any physical aging time in the range of time evaluated. The physical aging time shift factor appears to approach a horizontal asymptote after about six hours. This would suggest that if one is interested in

development of a *G** master curve after completion of the structural recovery process, then a wait of six hours at -20°C would be necessary. While that would be true for the quenched state at -20°C, in practice at least several frequency sweeps are generated over the temperature range of interest. Steric and physical hardening would occur at the various temperatures the frequency sweeps are performed. Generally, steric hardening is considered to occur above the glass transition temperature and physical hardening below the glass transition temperature. However, it is speculated that they are essentially the same, that is, in either case the material is moving towards a thermodynamic equilibrium.

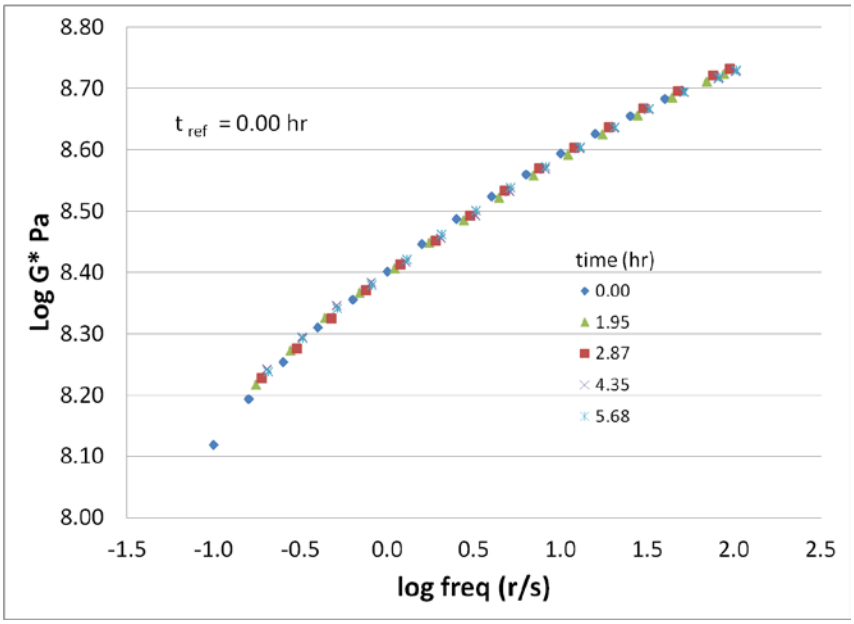

Figure 48. Graph. Physical aging frequency sweeps from figure 47 shifted to a reference physical aging time of zero hour.

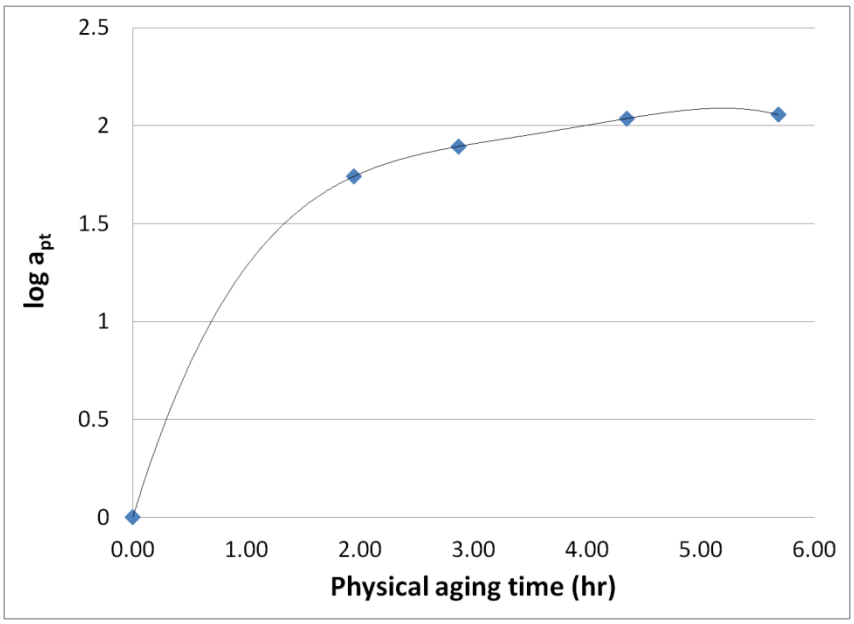

Figure 49. Graph. Physical aging time shift factor derived from figures 47 and 48. The points fitted with a polynomial for convenience, however a stretched exponential would probably provide a better fit.

The next step in this process would be to determine a parameter, intrinsic to the particular binder that would allow estimation of the equilibrium physical aging time shift factor (a_{ept}). It is speculated that the crossover modulus might be such a parameter. The crossover modulus may be related to molecular mobility, and molecular mobility is directly related to the rate at which the structural recovery process occurs.

However, at this point before proceeding with an attempt to correlate a_{ept} with crossover modulus or some other rheological parameter, it seems reasonable to ask if any of this discussion actually pertains to the actual physical hardening that occurs in the binder in the pavement in-service. After all, in terms of single event thermal cracking from a rapid cool down event or repeated thermal cycling, the end goal here is to develop a relaxation modulus master curve at the low PG +10°C temperature that approximates the actual binder condition in the pavement. The *G(t)* slope and magnitude at a reference temperature of PG +10°C and a time of 60 seconds would be used for a performance based specification, similar to the current bending beam rheometer (BBR) test and specifications based on the BBR inverse creep compliance curve (creep stiffness).

Most of the physical hardening research performed over the last 20 years in the asphalt field is based on BBR and to a much lesser extent torsion bar rheology. In terms of comparing the physical hardening that occurs in the BBR to 4-mm DSR, there are some distinct differences that should be noted. For example, the BBR beam is unconstrained and can change volume unhindered, whereas with 4-mm plate DSR the specimen is laterally constrained. Also, with BBR the beam is left essentially quiescent during the test, while the 4-mm plate DSR specimen is subjected to oscillatory shear.

Physical Hardening and Thermal Stress Build-up during Cooling

One way to evaluate the relationship between the physical hardening that occurs during a typical low temperature 4-mm DSR test and the actual physical hardening that occurs in the binder in the pavement is to use the Thermal Stress Restrained Specimen Test (TSRST) as a surrogate for the physical hardening that would occur in the pavement. The Thermal Stress Restrained Specimen Test (TSRST) is designed to measure the tensile stress in a specimen as it is cooled at a constant rate while being restrained from contracting. Load cell output during cool down can be used to determine the thermal stress build-up during cool down, and the coefficient of thermal expansion/contraction.

Recently, asphalt from a TSRST specimen was recovered and the asphalt low and intermediate temperature rheological properties were determined using 4-mm DSR. An estimated thermal stress build-up in a mix with the recovered asphalt was compared to the measured TSRST thermal stress as shown in figure 50 [Farrar et al. 2013b]. The two curves are remarkably similar.

No adjustments in terms of physical hardening were made to the 4-mm DSR data. However, there is little doubt that physical hardening was occurring during the 4-mm DSR test. Since the two curves in figure 50 are surprisingly close, it suggests the physical hardening that occurred during the 4-mm DSR test is similar to the physical hardening that occurred during the TSRST.

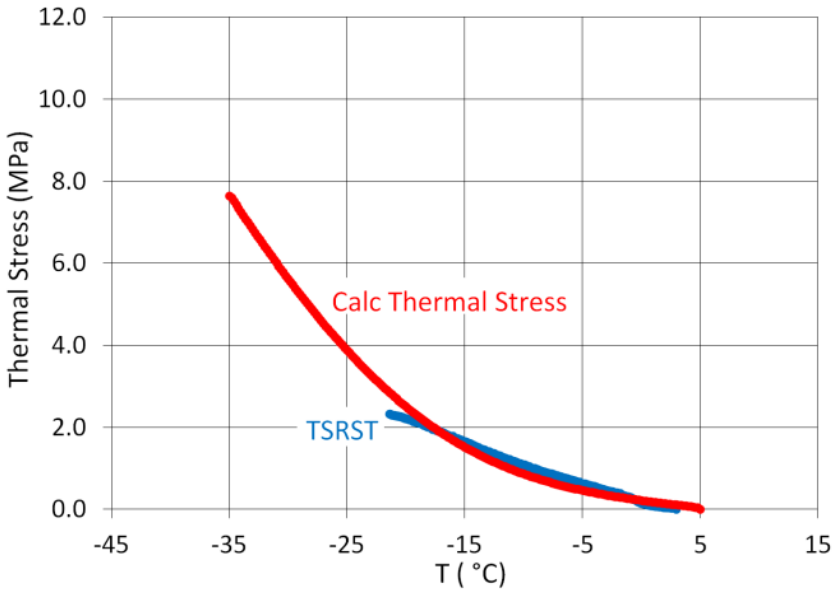

Figure 50. Graph. Comparison calculated and TSRST thermal stress build-up.

Torsion Bar versus 4-mm DSR

A series of torsion bar and 4-mm DSR tests were performed on an RTFO/PAV aged asphalt from the Rochester, MN, comparative test site. The asphalt from the test site is designated as MN1-5, and is an unmodified PG 58 – 28. The asphalt was derived from a blend of Venezuelan crude.

The tests were performed on an ARES rheometer. Spring loaded fixtures were used that did not require the use of end clips on the torsion bar specimen. Several thermal regimes for the torsion bar and 4 mm plate DSR specimens were tried, but regardless of the thermal regime there was typically a pronounced difference (significantly greater than 10%) between the torsion bar and 4 mm plate results. An example of the difference is shown in figure 51. The effect of measurement errors of the torsion bar's width and thickness were considered, but did not appear to be a major factor that could account for the observed differences.

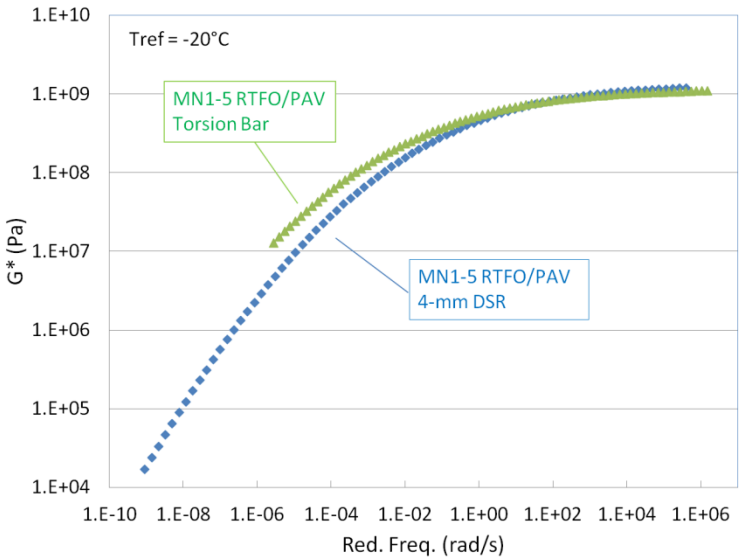

Figure 51. Graph. RTFO/PAV aged MN1-5 asphalt binder.

Figure 51 shows that G* collected on a DSR at low temperatures using 4 mm parallel plates was considerably lower in magnitude than G* collected using the torsion bar geometry. A suggestion was made that the actual temperature of the torsion bar was lower than read by the rheometer. This turned out to be true. A NIST-traceable resistance temperature detector **(**RTD) was attached to a torsion bar at the top middle and bottom, and the RTD output was compared with the rheometer platinum resistance thermometer (PRT) output. The rheometer PRT measurements were on average 2.1°C higher than the RTD. The gradient from top to bottom of the torsion bar was ± 0.1°C.

The torsion bar data collected was manually shifted along the frequency axis to determine the shift factor (a_T) as a function of temperature. The following 2nd order polynomial fit the data very well with a correlation coefficient of 0.99.

$$Log\ a_T = 0.0067 - 0.158(T - T_o) + 0.002015(T - T_o)^2$$

Figure 52. Equation. Estimated temperature shift factor.

where T is the measurement temperature and T_O is the reference temperature, T_O = -2.5°C in this case. The shift factor was then used to correct the temperature of the torsion bar data to agree with the temperatures used to collect the DSR parallel plate data (0, -10, -20 and -30°C). Figures 53 through 56 illustrate the dramatic effect that correcting the torsion data temperature has on reducing the discrepancy with the 4-mm plate data. Second-order polynomial fits were used to compare the data at the same frequencies to determine the error between measurement sets. The error data is in table 5. Also in table 5 are the results from annealing a 4 mm plate sample. The sample was annealed at -20°C for four hours prior to starting measurements at 0, -10 and -20°C, in that order. This was done to simulate the freezer storage that occurred with the torsion bars prior to loading in the rheometer at 0°C. This increased the 4 mm plate data slightly. Figures 57 through 59 illustrate this as well.

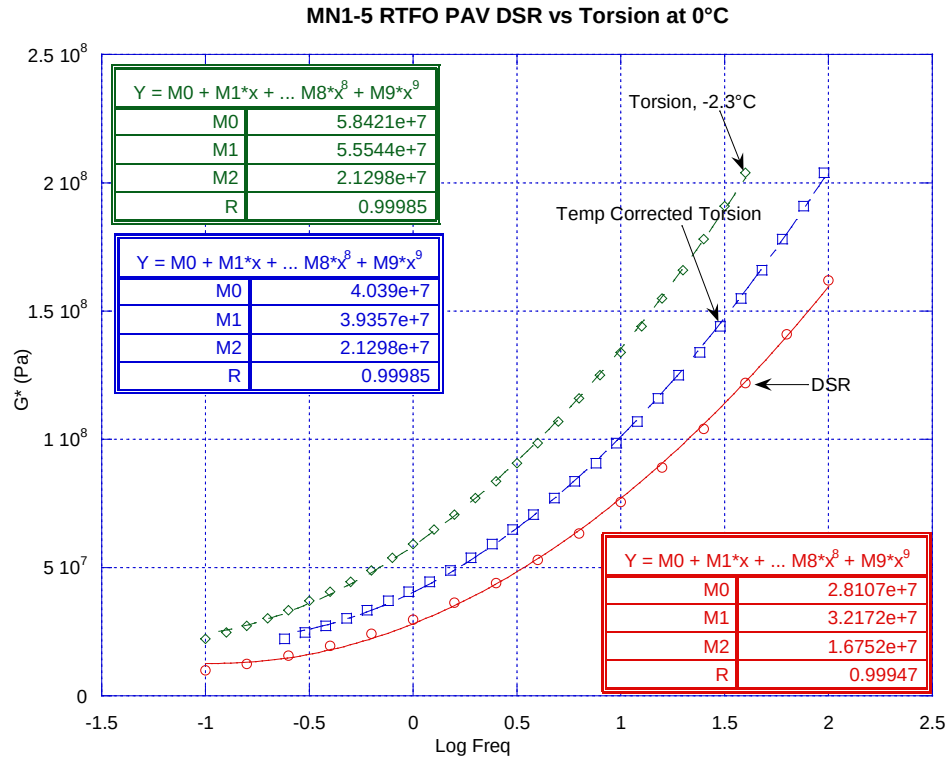

Figure 53. Graph. MN1-5 RTFO PAV DSR vs. Torsion at 0°C.

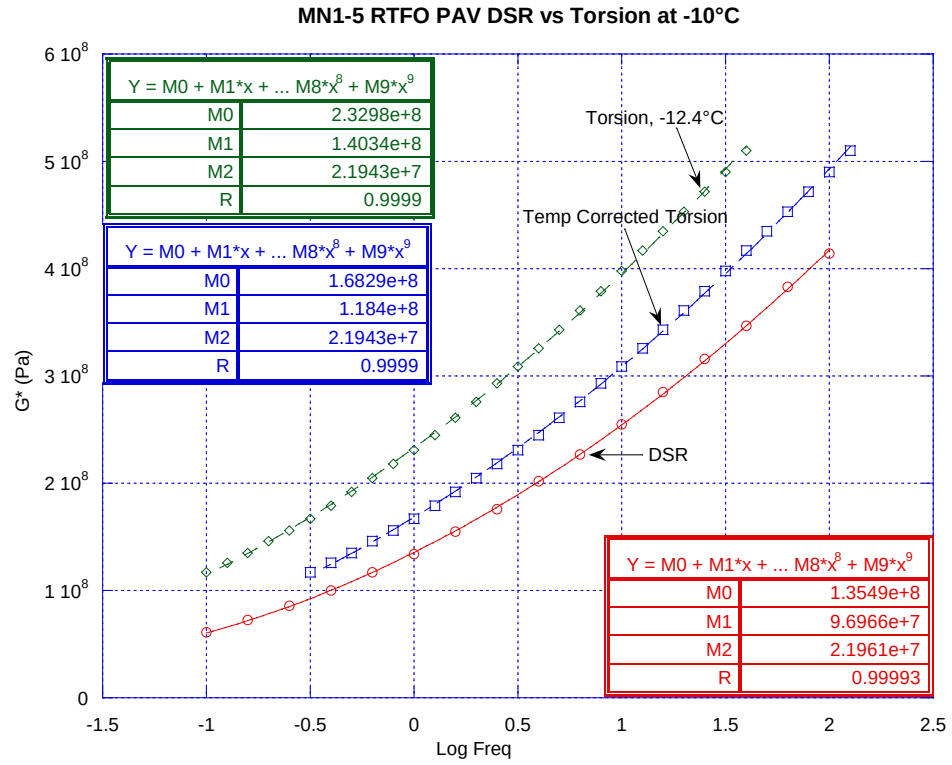

Figure 54. Graph. MN1-5 RTFO PAV DSR vs. Torsion at -10°C.

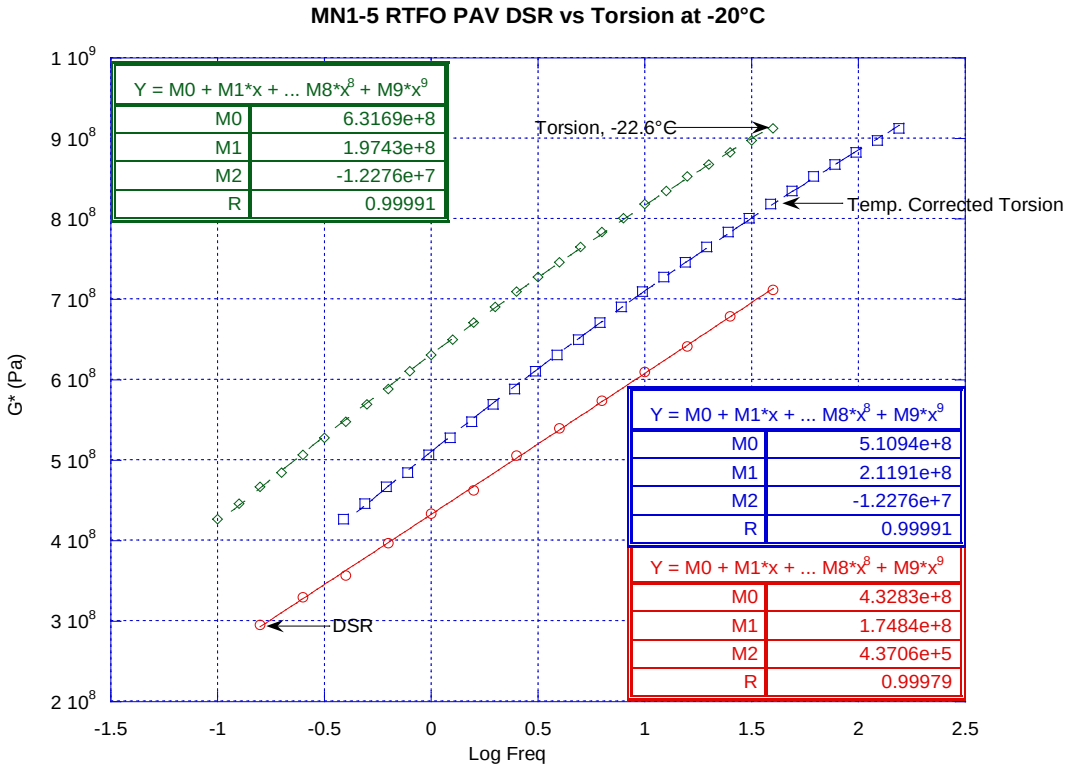

Figure 55. Graph. MN1-5 RTFO PAV DSR vs. Torsion at -20°C.

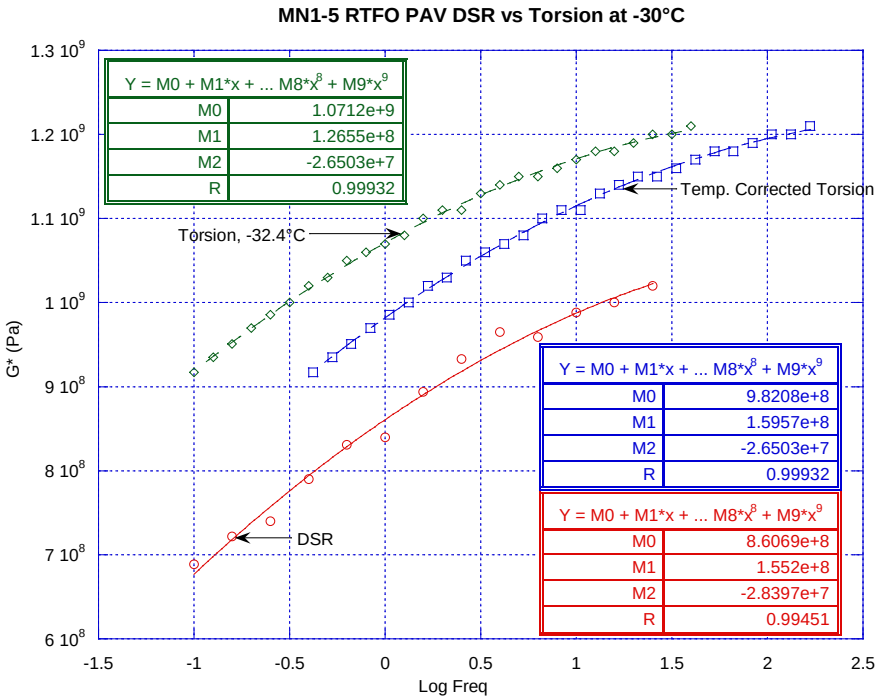

Figure 56. Graph. MN1-5 RTFO PAV vs. Torsion at -30°C.

Table 5. % Errors comparing DSR with torsion bar data.

Temp (°C)	0	-10	-20	-30
Uncorrected Torsion Data	40 - 55	33 - 44	23 - 34	15 - 22
Temp Corrected Torsion Data	23 - 36	17 - 20	13 - 15	11 - 13
Annealed DSR	21 - 22	12 - 13	14 - 15	---

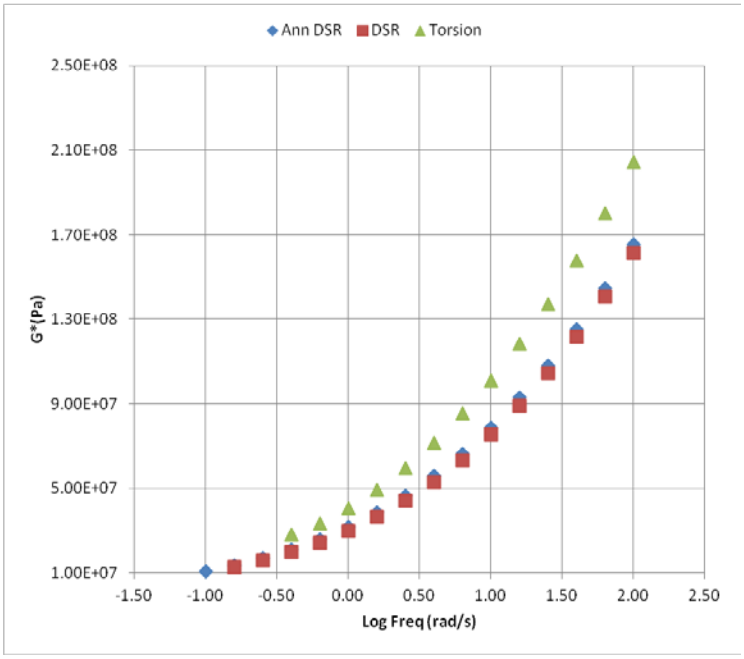

Figure 57. Graph. MN1-5 RTFO PAV DSR Torsion at 0°C.

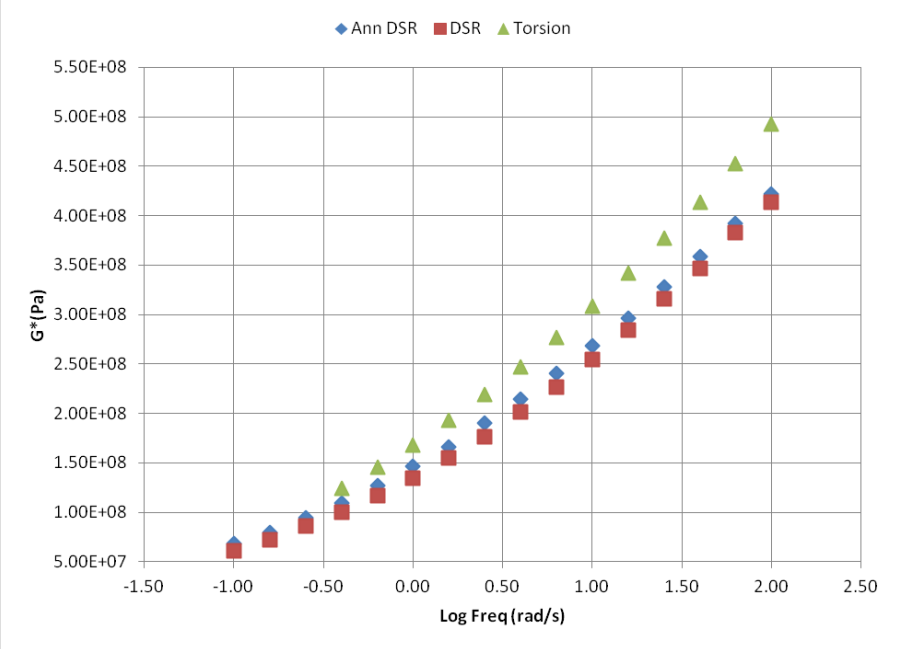

Figure 58. Graph. MN1-5 RTFO PAV DSR vs. Torsion at -10°C.

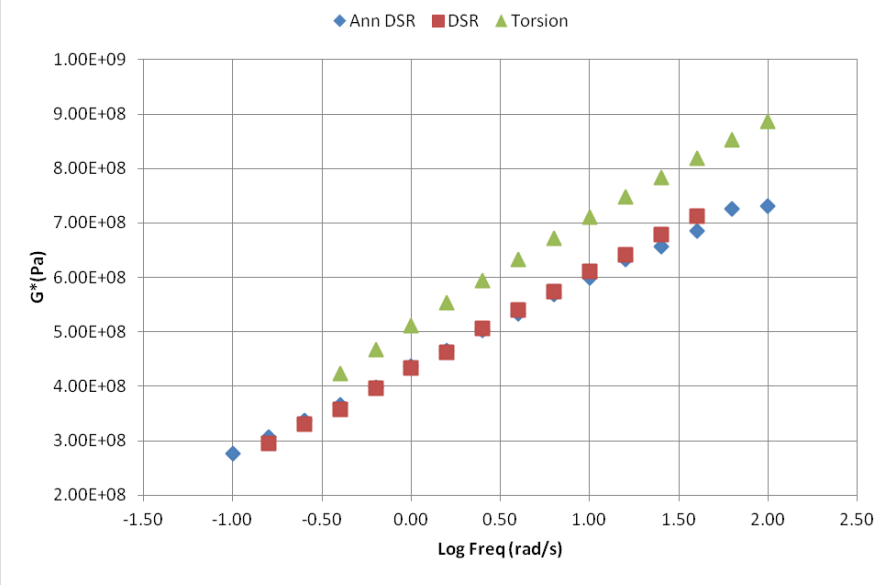

Figure 59. Graph. MN1-5 RTFO PAV DSR vs. Torsion at -20°C.

SUMMARY AND CONCLUSIONS

This report documents the resolution of the instrument compliance issue and other related issues in order to develop a DSR method that is an alternative to BBR and suitable for specification purposes. The DSR method with compliance correction is referred to in this report as "4-mm DSR." However, the instrument compliance correction can be applied to any plate diameter from 4 to 8 mm. The lower limit is due to difficulty in sample trimming and the upper limit is necessary to limit the total instrument compliance.

Important observations and conclusions are presented below:

- In addition to application as an alternative to BBR, 4-mm DSR has led to a number of new and novel spin-off technologies and applications such as the Universal Simple Aging Test (USAT).

- A simple alternative to the solid rod fixture for measuring instrument compliance was developed. It was found that Superglue can be used to chemically weld the plates together creating in effect a solid rod. After gluing the plates together the procedure to measure the instrument compliance is the same as for the solid rod.

- The frequency dependence when measuring instrument compliance can be significant for certain types of rheometers. A possible solution to the frequency dependency issue is to modify the instruments software algorithm to adjust the compliance correction for frequency using for example an exponential function.

- A mathematical method for correcting errors in the dynamic moduli $G'(\omega)$ and $G''(\omega)$ due to instrument compliance was developed and can be used when real-time online

instrument compliance correction by the rheometer software is unavailable or to check the instrument compliance correction.

- Low-temperature rheological parameters such as BBR m-value and creep stiffness can be estimated through a correlation with 4-mm DSR. The slope and magnitude of the shear stress relaxation modulus *G(t)* master curve at 60 seconds and 10°C above the true low PG grading are correlated with the corresponding *S*(*t*) and m-values at 60 seconds and 10°C above the true low PG grading temperature from BBR measurements.

- The ARES is much less susceptible to inertia effects compared to the ARG-2. Generally, inertia effects on the ARES are negligible for a test frequency below 100 rad/s.

- In terms of physical hardening effects, it was found that 4-mm DSR provides estimates of BBR m-value and creep stiffness values that are comparable to standard BBR, even for asphalts with considerable crystalline fraction such as AAM-1.

- Based on the remarkable similarity between the measured TSRST thermal stress build-up and calculated thermal stress using 4-mm DSR data, it appears the physical hardening that occurs during the 4-mm DSR test is similar to the physical hardening that occurs during the TSRST. Note: this conclusion is based on very limited data.

ACKNOWLEDGMENTS

The authors gratefully acknowledge the Federal Highway Administration, U.S. Department of Transportation, for financial support of this project under contract no. DTFH61-07D-00005.

DISCLAIMER

This document is disseminated under the sponsorship of the Department of Transportation in the interest of information exchange. The United States Government assumes no liability for its contents or use thereof.

The contents of this report reflect the views of Western Research Institute which is responsible for the facts and the accuracy of the data presented herein. The contents do not necessarily reflect the official views of the policy of the Department of Transportation.

REFERENCES

Anderson, D. A., and M. O. Marasteanu, 1999, Physical Hardening of Asphalt Binders Relative to Their Glass Transition Temperatures. In *Transportation Research Record: Journal of the Transportation Research Board*, No. 1661, Transportation Research Board of the National Academies, Washington, D.C., pp. 27-34.

Anderson, D. A., M. O. Marasteanu, and Y. Liu, 1999, Dilatometric Measurements of Glass Transition Temperatures. In *Transportation Research Record, Journal of the Transportation Research Board,* No.1661, Transportation Research Board of the National Academies, Washington, D.C.

Bahia, H.U., and D.A. Anderson, 1993, Glass Transition Behavior and Physical Hardening of Asphalt Binders. *Journal of Association of Asphalt Paving Technologists,* Vol. 62.

Bahia, H., M. Zeng, and K. Nam, 2000, Consideration of Strain at Failure and Strength in Prediction of Pavement Thermal Cracking. *Journal of the Association of Asphalt Pavement Technologists,* 69: 497-540.

Christensen, R. M., 1982, *Theory of Viscoelasticity – an Introduction*, Academic Press, New York.

Christensen, D. W., and D. A. Anderson, 1992, Interpretation of mechanical test data for paving grade asphalt cements. *Journal of the Association of Asphalt Paving Technologists,* 61: 67-116.

Farrar, M., R. W. Grimes, T. F. Turner, and J-P. Planche, 2015a, The Universal Simple Aging Test (USAT) and Low Temperature Performance Grading Using Small Plate Dynamic Shear Rheometry: An Alternative to Standard RTFO, PAV, and BBR for HMA and WMA. Technical white paper FP14 prepared by Western Research Institute for the Federal Highway Administration, Contract No. DTFH61-07-D-00005, Fundamental Properties of Asphalts and Modified Asphalts, III, March 2014.

Farrar, M. J., R. W. Grimes, S. Wiseman, and J. P. Planche, 2015b, Asphalt Pavement – Micro-sampling and Micro-extraction Methods. Technical white paper FP 09 prepared by Western Research Institute for the Federal Highway Administration, Contract DTFH61-07-D-00005, Fundamental Properties of Asphalts and Modified Asphalts, III, September 2013 March 2015.

Farrar, M. J., J-P. Planche, R. W. Grimes, and Q. Qin, 2014a, The Universal Simple Aging Test (USAT): Simulating Short- and Long Term Hot and Warm Mix Oxidative Aging in the Laboratory. Presented at the 2014 ISAP conference at NCSU, Raleigh, NC, June 2014, in press.

Farrar, M. J., Q. Qin, R. W. Grimes, J-P. Planche, R. Boysen, J. Loveridge, S. Salmans, and A. O. Cookman, 2014b, Field Sampling and Testing of Death Valley Chip Seal Emulsion Residue: A Case Study. *Transportation Research Circular*, Number E-C182 January 2014.

Farrar, M. J., S. L. Salmans, and J-P. Planche, 2013a, Recovery and Laboratory Testing of Asphalt Emulsion Residue: Application of Simple Aging Test and 4-mm Dynamic Shear Rheometer Test. *Transportation Research Record, Journal of the Transportation Research Board, No. 2370*, 69-75.

Farrar, M. J., E. Y. Hajj, J-P. Planche, and M. Z. Alavi, 2013b, A method to estimate the thermal stress build-up in an asphalt mixture from a single cooling event. *Road Materials and Pavement Design*, 14, sup1: 201-211.

Farrar, M. J., R. W. Grimes, C. Sui, J-P. Planche, S-C. Huang, T. F. Turner, and R. Glaser, 2012, Thin Film Oxidative Aging and Low Temperature Performance Grading Using Small Plate Dynamic Shear Rheometry: An Alternative to Standard RTFO, PAV, and BBR. *Proc.*, 5th Eurasphalt & Eurobitume Congress, Istanbul, June 13-15, 2012.

Ferry, J.D., 1961, *Viscoelastic Properties of Polymers*, New York: Wiley, p. 467.

Franck, A. J., 2006, TA Instruments, *Understanding Instrument Compliance Correction in Oscillation*, APN013, November 2006 Version 1.

Franck, A. J. 2005, "Instrument Inertia Correction during Dynamic Mechanical Testing," APN 006, TA Instruments.

Gordon, G. V., and M. T. Shaw, 1994, *Computer Programs for Rheologists*, Hanser/Gadner Publ.

Gottlieb, M., and C. W. Macosko, 1982, The effect of instrument compliance on dynamic rheological measurements. *Rheol. Acta*, 21, 90.

Hutcheson, S. A., 2009, Personal communication (email) with Stephen A. Hutcheson, Wednesday, 6/10/09.

Hutcheson, S. A, 2008, "Evaluation of Viscoelastic Materials: The Study of Nanosphere Embedment Into Polymer Surfaces and Rheology of Simple Glass Formers using a Compliant Rheometer, a Dissertation in Chemical Engineering submitted to the Graduate Faculty of Texas Tech University in Partial Fulfillment of the Requirements for the Degree of Doctor of Philosophy, August 2008.

Hutcheson, S. A., and G. B. McKenna, 2008, The Measurement of Mechanical Properties of Glycerol, m-toluidine, and Sucrose Benzoate under Consideration of Corrected Rheometer Compliance: An In-depth Study and Review. *J. Chem. Phys.*, 129, 074502-1-07452-14.

Jacobs, J. A., and T. F. Kilduff, 2001, *Engineering Materials Technology: Structures,* 41 *Processing, Properties, and Selection*. Prentice-Hall, Englewood Cliffs, NJ.

Kriz, P., 2009, "Glass Transition and Physical Hardening of Asphalts." A thesis submitted to the Faculty of Graduate Studies, Department of Civil Engineering, University of Calgary, March 2009.

Mackay, M. E., and P. J. Halley, 1991, Technical Note: Angular Compliance Error in Force Rebalance Torque Transducers. *Journal of Rheology*, 35: 1609-1614.

Marasteanu, M., and D. Anderson, 1996, Time-Temperature Dependency of Asphalt Binders-An Improved Model. *Journal of Association of Asphalt Paving Technologists,* Vol. 65.

Pink, H. S., R. E. Merz, and D. S. Bosniack. 1980, Asphalt Rheology: Experimental Determination of Dynamic Moduli at Low Temperature. *Journal of Association of Asphalt Paving Technologists*, 49: 64-94.

Planche, J. P., P. M. Claudy, J. M. Létoffé, and D. Martin, 1998, Using Thermal Analysis Methods to Better Understand Asphalt Rheology. *Thermochimica Acta*, 324: 223-227.

Qin, Q., M. Farrar, A.T. Pauli, and J. J. Adams, 2014a, Morphology, thermal analysis and rheology of Sasobit modified warm mix asphalt binders. *Fuel*, 115: 416-425, 2014.

Qin, Q., A. T. Pauli, M. J. Farrar, 2014b, Microstructure - Property Relationships of Sasobit Modified Warm Mix Asphalts, Presented at the 2014 ISAP conference at NCSU, Raleigh, NC, June 2014, in press.

Qin, Q., M. Farrar, T. F. Turner, and J-P. Planche, 2015, Characterization of the Effects of Wax (Sasobit®) on Asphalt Binder. Technical white paper FP13 prepared by Western Research Institute for the Federal Highway Administration, Contract No. DTFH61-07-D-00005, Fundamental Properties of Asphalts and Modified Asphalts, III, March 2015.

Reinke, G. H., and S. L. Engber, 2002, Impact of Factors Affecting Determination of Glass Transition Temperature Using a Dynamic Shear Rheometer. *Journal of Association of Asphalt Paving Technologists*, 71: 471-493.

Rides, M., and A. Olusanya, Appendix, Compliance Correction, Olusanya, A., "A Comparison of Techniques for Monitoring the Cure of Adhesives," MTS Adhesives Project 5, Measurements for Optimising Adhesives Processing Report 10, NPL Report CMMT(B104) National Physical Laboratory, Teddington, Middlesex, UK, ISSN 1361-4061, November 1996.

Salmans, S., M. Farrar, C. Sui, and J-P. Planche, 2015, Emulsions: Recovery, Aging, and Rheological Testing. Technical white paper FP18 prepared by Western Research Institute for the Federal Highway Administration, Contract No. DTFH61-07-D-00005, Fundamental Properties of Asphalts and Modified Asphalts, III, March 2015.

Schröter, K., S. A. Hutcheson, X. Shi, A. Mandanici, and G. B. McKenna, 2006, Dynamic Shear Modulus of Glycerol: Corrections Due to Instrument Compliance. *Journal of Chemical Physics*, 125: 214507.

Shi, X., 2004, Rheology of Complex Fluids: Mechanical Hole Burning Spectroscopy and Organic Complex Fluids, Ph.D. dissertation, Texas Tech University.

Sui, C., M. J. Farrar, P. M. Harnsberger, W. H. Tuminello, and T. F. Turner, 2011, New Low-Temperature Performance-Grading Method Using 4-mm Parallel Plates on a Dynamic Shear Rheometer. In *Transportation Research Record: Journal of the Transportation Research Board*, No. 2207, Transportation Research Board of the National Academies, Washington, D.C., 43-48.

Sui, C., M. J. Farrar, W. H. Tuminello, and T. F. Turner, 2010, New Technique for Measuring Low-Temperature Properties of Asphalt Binders with Small Amounts of Material. In *Transportation Research Record: Journal of the Transportation Research Board*, No. 2179, Transportation Research Board of the National Academies, Washington, D.C., 23-28.

Tabatabaee, H. A., R. Velasquez, and H. U. Bahia, 2012, Predicting low temperature physical hardening in asphalt binders. *Construction and Building Materials*, 34: 162-169.

APPENDIX

Standard Method of Test for

Determining the Low Temperature Rheological Properties of Asphalt Binder Using a Dynamic Shear Rheometer (DSR)

AASHTO Designation: T XXX-12

1. SCOPE

1.1. This test method covers the determination of the dynamic shear modulus and phase angle of asphalt binder when tested in dynamic (oscillatory) shear using parallel plate test geometry at low (-40 to 0°C) temperature. This test method is intended for determining the linear viscoelastic properties of asphalt binders as required for specification testing and is not intended as a comprehensive procedure for the full characterization of the viscoelastic properties of asphalt binder.

1.2. This standard is appropriate for unaged material, and material aged in accordance with T 240 and R 28.

1.3. *This standard may involve hazardous materials, operations, and equipment. This standard does not purport to address all of the safety concerns associated with its use. It is the responsibility of the user of this procedure to establish appropriate safety and health practices and to determine the applicability of regulatory limitations prior to use*.

2. REFERENCED DOCUMENTS

2.1. *AASHTO Standards*:

- M 315 Standard Test Method for Determining the Rheological Properties of Asphalt Binder Using a Dynamic Shear Rheometer
- M 320, Performance-Graded Asphalt Binder
- R 28, Accelerated Aging of Asphalt Binder Using a Pressurized Aging Vessel (PAV)
- R 29, Grading or Verifying the Performance Grade (PG) of an Asphalt Binder
- T 40, Sampling Bituminous MaterialsT315, Determining the Rheological Properties of Asphalt Binder Using a Dynamic Shear Rheometer (DSR)
- T 240, Effect of Heat and Air on a Moving Film of Asphalt Binder (Rolling Thin-Film Oven Test)

2.2. *ASTM Standards*:

- D 7175, Standard Test Method for Determining the Rheological Properties of Asphalt Binder Using a Dynamic Shear Rheometer

3. TERMINOLOGY

3.1. *Definitions*:

3.1.1. *asphalt binder*—an asphalt-based cement that is produced from petroleum residue either with or without the addition of non-particulate organic modifiers.

3.2. *Descriptions of Terms Specific to This Standard*:

3.2.1. *annealing*—heating the binder until it is sufficiently fluid to remove the effects of steric hardening.

3.2.2. *complex shear modulus (G*)*—ratio calculated by dividing the absolute value of the peak-to-peak shear stress, τ, by the absolute value of the peak-to-peak shear strain, γ.

3.2.3. *calibration*—process of checking the accuracy and precision of a device using NIST-traceable standards and making adjustments to the device where necessary to correct its operation or precision and accuracy.

3.2.4. *dummy test specimen*—a specimen formed between the dynamic shear rheometer (DSR) test plates from asphalt binder or other polymer to measure the temperature of the asphalt binder held between the plates. The dummy test specimen is used solely to determine temperature corrections.

3.2.5. *loading cycle*—a unit cycle of time for which the test sample is loaded at a selected frequency and stress or strain level.

3.2.6. *phase angle (δ)*—the angle in radians between a sinusoid ally applied strain and the resultant sinusoidal stress in a controlled-strain testing mode, or between the applied stress and the resultant strain in a controlled-stress testing mode.

3.2.7. *loss shear modulus (G″)*—the complex shear modulus multiplied by the sine of the phase angle expressed in degrees. It represents the component of the complex modulus that is a measure of the energy lost (dissipated during a loading cycle).

3.2.8. *storage shear modulus (G′)*—the complex shear modulus multiplied by the cosine of the phase angle expressed in degrees. It represents the in-phase component of the complex modulus that is a measure of the energy stored during a loading cycle.

3.2.9. *parallel plate geometry*—refers to a testing geometry in which the test sample is sandwiched between two relatively rigid parallel plates and subjected to oscillatory shear.

3.2.10. *oscillatory shear*—refers to a type of loading in which a shear stress or shear strain is applied to a test sample in an oscillatory manner such that the shear stress or strain varies in amplitude by about zero in a sinusoidal manner.

3.2.11. *linear viscoelastic*—within the context of this specification refers to a region of behavior in which the dynamic shear modulus is independent of shear stress or strain.

3.2.12. *portable thermometer*—is an electronic device that consists of a temperature detector (probe containing a thermocouple or resistive element), required electronic circuitry, and readout system.

3.2.13. *reference thermometer*—a NIST–traceable liquid-in-glass or electronic thermometer that is used as a laboratory standard.

3.2.14. *temperature correction*—difference in temperature between the temperature indicated by the DSR and the test specimen as measured by the portable thermometer inserted between the test plates.

3.2.15. *thermal equilibrium*—is reached when the temperature of the test specimen mounted between the test plates is constant with time.

3.2.16. *verification*—process of checking the accuracy of a device or its components against an internal laboratory standard. It is usually performed within the operating laboratory.

3.2.17. *steric hardening*—see molecular association.

3.2.18. *physical hardening*— structural relaxation below the glass transition temperature.

3.2.19. *normal force*— the force perpendicular to the surface of the parallel plates.

3.2.20. *molecular association*—a process where associations occur between asphalt binder molecules during storage at ambient temperature. Often called steric hardening in the asphalt literature, molecular associations can increase the dynamic shear modulus of asphalt binders. The amount of molecular association is asphalt specific and may be significant even after a few hours of storage.

4. SUMMARY OF TEST METHOD

4.1. Test specimens 1.75 mm by 4 mm or 2.00 mm by 8 mm are formed between 4 and 8 mm diameter parallel metal plates, respectively. During testing, one of the parallel plates is oscillated with respect to the other at pre-selected frequencies and rotational deformation amplitudes (strain control) (or torque amplitudes (stress control). A strain or stress sweep is required at each isotherm to insure testing in the linear viscoelastic range.

4.2. The test specimen is maintained at the test temperature to within ±0.1°C by positive heating and cooling of the upper and lower plates or by enclosing the upper and lower plates in a thermally controlled environment or test chamber. Test temperatures are between -40 and 0°C.

4.3. The complex modulus (G^*) and phase angle (δ) are calculated automatically as part of the operation of the rheometer using proprietary computer software supplied by the equipment manufacturer.

5. SIGNIFICANCE AND USE

5.1. The test method is a significant benefit to low temperature rheological testing in several ways: (1) the method includes a procedure to measure instrument compliance; (2) testing as low as -40°C is achievable by way of a correction for machine compliance; (3) when using 4mm diameter plates, only 25mg of binder is required for a test (note: in actual practice 150 mg for sample loading and trimming is required, but that is about 100 times less than required under AASHTO T313 to prepare 1 beam) ; (4) a commercial dynamic shear rheometer is a more precise instrument than a bending beam rheometer; (5) intermediate test temperatures are achievable: for 4 mm and 8 mm diameter plates, approximately 0 to 30°C and 0 to 45°C, respectively.

5.2. Test temperatures are related to the low temperatures experienced by the pavement in the geographical area for which the asphalt binder is intended to be used. Master curves of G* and δ curves at selected temperatures can be developed employing time-temperature superposition. The master curves can be used to calculate low temperature performance-related criteria in accordance with M 320.

6. APPARATUS

6.1. The dynamic shear rheometer, environmental chamber and control and data acquisition system shall meet the requirements of T315. Test plates shall be 4.00 ± 0.01 mm or 8.00 ± 0.01mm in diameter, stainless steel or aluminum with smooth ground surface. In addition, the rheometer shall be equipped with a normal force sensor.

Note 1—When measuring low temperature properties by DSR, errors due to instrument compliance need to be corrected. For older DSR's, without updated software to do the real-time online instrument compliance corrections, one can use the method in Appendix A1. For updated DSR the real-time online instrument compliance correction is made by pre-inputting the instrument compliance value into the software. Regardless of the way the correction is performed, the value of instrument compliance is the most important factor. How to measure the instrument compliance is covered in Appendix A2.

7. HAZARDS

7.1. Standard laboratory caution should be used in handling the hot asphalt binder when preparing test specimens.

8. PREPARATION OF APPARATUS

8.1. Prepare the apparatus for testing in accordance with the manufacturer's recommendations. Specific requirements will vary for different DSR models and manufacturers.

8.2. Inspect the surfaces of the test plates and discard any plates with jagged or rounded edges or deep scratches. Clean any asphalt binder residue from the plates with an organic solvent such as mineral oil, mineral spirits, a citrus-based solvent, or toluene. Remove any remaining solvent residue by wiping the surface of the plates with a cotton swab or a soft cloth dampened with acetone. If necessary, use a dry cotton swab or soft cloth to ensure that no moisture condenses on the plates.

8.3. Mount the cleaned and inspected test plates on the test fixtures and tighten firmly.

9. VERIFICATION AND CALIBRATION

9.1. Verify the DSR and its components at least every six months and when the DSR or plates are newly installed, when the DSR is moved to a new location, or when the accuracy of the DSR or any of its components is suspect in accordance with T315.

10. PREPARING TEST SAMPLES

10.1. Anneal the asphalt binder in a forced draft oven at 70°C. For relatively large amounts of material such as an RTFO-PAV aged sample (50 g) in a standard PAV pan, an annealing time of about 30 min. is required. For smaller amounts of binder (<10 g) only 15 minutes is required. For very small amounts (<`1 g) an argon blanket should be used to prevent oxidation.

10.2. While the sample is being annealed, carefully clean and dry the surfaces of the test plates so that the specimen will adhere to both plates uniformly and strongly. Heat the rheometer oven or Peltier plates to 30°C and stabilize at this temperature for about 20 min. Zero the gap in accordance with [Preparation of Apparatus].

10.3. Move the plates apart to 5 mm and preheat the plates to ~ 60°C to improve the adhesion between the asphalt and the plates.

10.4. Transfer the annealed hot asphalt to the lower fixed plate using a metal spatula or other tools.

10.5. Immediately after the transferring, move the test plates together until approaching the desired testing gap plus the gap closure to create the bulge: (1) 4 mm diameter plates - the desired testing gap is 1.75 mm and the closure gap for the bulge is 0.120

mm; (2) 8 mm diameter plates - the desired testing gap is 2.00 mm and the closure gap for the bulge is 0.150 mm).

10.6. Trim excess asphalt binder by moving a heated trimming tool around the edges of the plates so that the asphalt binder is flush with the outer diameter of the plates. Use a magnifying lens, external light source and mirror to observe the entire surface of the trimmed sample and insure a uniform trimmed surface.

10.7. Close the chamber door and heat the sample to the preheating temperature (~60°C) for about 5 min.

10.8. Cool the system down to 30°C and decrease the gap by the amount of closure gap (0.120 mm for 4 mm plates, and .150 mm for 8 mm plats).

10.9. Condition the sample at 30°C for 20 min.

11. PROCEDURE

11.1. After conditioning the specimen for 20 minutes at 30°C the measuring system shall then be cooled to the target testing temperature and stabilized at the testing temperature for 20 min when testing binder for compliance with M 320.

Note 2—When changing temperature, the metallic rheometer parts and measurement geometries thermally expand or contract causing an expansion or contraction of the gap. The change in the gap due to system thermal expansion or contraction must be compensated for to keep the gap constant. To compensate and keep the gap constant a correction factor must be determined and the gap adjusted for changes in temperature as discussed Appendix A3.

Note 3—Even with the gap correction performed manually or automatically to compensate for system thermal expansion or contraction, the sample will expand or contract with change in temperature causing changes in the sample shape and generation of normal force. This is particularly true at test temperatures close to or below the glass transition temperature of the test materials. In some cases the build-up in thermal stress may be sufficient to damage the normal force transducer. To keep a uniform sample shape as well as to avoid machine damage, the moving plate has to be adjusted to compensate for build up in normal force due to sample expansion or contraction. The normal force should be monitored when changing temperature and the gap adjusted beyond the necessary adjustment for system expansion or contraction to keep the normal force at zero. In no case should the normal force exceed 20 grams during cooling or heating. If performed manually, this adjustment in the gap to keep the normal force at zero causes a very slight error in the gap, but it is small enough that it can be neglected. Some rheometers can maintain the normal force at zero and any slight change in the gap is accounted for eliminating the slight error when the correction is manually performed.

11.2. After cooling to the test temperature, which typically takes about 3 to 5 minutes, condition the sample at the test temperature for 20 minutes. A specific time of 20

minutes is specified to keep the extent of physical hardening at low temperature uniform during testing.

11.3. After the 20 minute conditioning period, perform a strain or stress sweep test (a strain sweep if the rheometer is strain controlled or a stress sweep if the rheometer is stress controlled) to determine the linear viscoelastic region and select an appropriate linear stain. After the strain or stress sweep test is finished, a plot of G*, G' and G" should be developed in the instrument software. Examine the plot for regions in which all three of these variables form a flat (slope of 0) line. It is in this linear viscoelastic region of all three variables where the percent strain or stress for the frequency sweep should be selected. In some cases, the entire plot may be linear, only a small region linear, or no linearity may be observed. Some instruments can be programmed to perform the strain or stress sweep and select an appropriate strain or stress level (usually the mid-point of the linear region) automatically.

11.4. Perform a frequency sweep test in a frequency range of 0.1 to 50 rad/s using the linear strain or stress determined in step 11.3. There will be 15 steps in the frequency sweep as shown in Table 1.

Table 1—Frequency Sweep Steps

Frequency rad/s														
0.10	0.15	0.25	0.39	0.63	1.00	1.58	2.51	3.98	6.31	10.00	15.85	25.12	39.81	50.00

11.5. Cool the sample to the next isotherm repeating steps 11.2 through 11.4.

12. INTERPRETATION OF RESULTS

12.1. The two frequency sweeps performed at, PG+10°C and PG+20°, are used to develop a storage modulus G'(ω) master curve using time-temperature superposition at a reference temperature of PG+10°C. The relaxation modulus G(t) curve is then determined thru interconversion. The slope (m_r) and magnitude G(t) for M 320 are determined from the relaxation modulus master curve at 60 seconds. Appendix A4 provides further discussion and an example of the process to determine m_r and G(t) at 60 seconds.

13. REPORT

13.1. **REPORT** TS-X T XXX-X AASHTO

13.2. Mr(60 sec) to one decimal place and G(60 sec) to the nearest whole number

14. PRECISION AND BIAS

14.1. To be determined upon results of inter-laboratory testing.

15. KEYWORDS

15.1. Dynamic shear rheometer; DSR; storage modulus; relaxation modulus, asphalt binder.

16. REFERENCES

16.1. Olusanya, A., "A Comparison of Techniques for Monitoring the Cure of Adhesives," MTS Adhesives Project 5, Measurements for Optimizing Adhesives Processing Report 10, NPL Report CMMT(B104) National Physical Laboratory, Teddington, Middlesex, UK, ISSN 1361-4061, November 1996.

16.2. Franck, A. J., TA Instruments, *Understanding Instrument Compliance Correction in Oscillation*, APN013, November 2006 Version 1.

16.3. Schröter, K., S. A. Hutcheson, X. Shi, A. Mandanici, and G. B. McKenna, Dynamic Shear Modulus of Glycerol: Corrections Due to Instrument Compliance. *J. Chem. Phys*., 125, 214507, 2006.

16.4. Hutcheson, S. A., and G. B. McKenna, The measurement of mechanical properties of glycerol, *m*-toluidine, and sucrose benzoate under consideration of corrected rheometer compliance: An in-depth study and review. *J. Chem. Phys*., 129, 074502, 2008.

16.5. Sui, C., M. J. Farrar, W. H. Tuminello, and T. F. Turner, New Technique for Measuring Low-Temperature Properties of Asphalt Binders with Small Amounts of Material. *Transportation Research Record 2179*, 23-28, 2010.

16.6. Christensen, R. M. *Theory of Viscoelasticity – an Introduction*, Academic Press, New York, 1982.

17. APPENDIXES

17.1. (Mandatory Information)

A1. INSTRUMENT COMPLIANCE CORRECTION

A1.1. *Scope:*

A1.1.1. This is a mathematical method for correcting errors due to instrument compliance and is applicable to the data collected on a DSR that does not have a real-time online instrument compliance correction function.

A1.2. *Mathematical methodology:*

For low temperature rheological measurements, the stiffness of the test material could be comparable to that of the instrument so instrument compliance can't be

neglected in order to obtain reliable results. The measured data has to be properly corrected by taking the instrument compliance into account.

In 1996, Rides and Olusanya proposed an instrument compliance correction for oscillatory shear rheometry (Olusanya 1996). Franck proposed a similar correction in 2006.

Schroter et al. (2006) and Hutcheson and McKenna (2008) demonstrated that error from not properly taking into account rheometer compliance can be quite significant and that the resulting inaccuracies in the determined mechanical properties can result in mistakes in material modeling, design, and theory.

Sui et al. (2010) were the first to apply an instrument compliance correction to asphalt binder low temperature oscillatory shear measurements (~ 5°C to -40°C) using parallel plate geometry.

A1.2.1. Dynamic data correction

When the rheological measurements are on stiff samples or at low temperatures, the actual measured angular displacement (θ_m) includes the sample angular displacement (θs) and the machine or tool angular displacement (θ_t).

$$\theta_m = \theta_s + \theta_t \quad (1)$$

The torsional stiffness K is related to the angular displacement θ and the torque M as follows:

$$K = \frac{M}{\theta} \quad (2)$$

Under the applied torque M,

$$\frac{1}{K_m} = \frac{1}{K_s} + \frac{1}{K_t} \quad (3)$$

Where K_m is the measured stiffness, K_s is the sample stiffness and K_t represents the machine or fixture tool stiffness.

By rearranging Equation (3), the sample stiffness can be obtained as

$$K_s = \frac{K_m K_t}{K_t - K_m} \quad (4)$$

To convert the torsional stiffness (K) into shear modulus (G), the geometry constant or the geometry conversion factor (k_g) needs to be introduced.

$$K = {}^{G}/_{k_g} \quad (5)$$

For example, for the parallel plate fixture geometry with plate radius R and gap between plates of h,

$$k_g = \frac{2h}{\pi R^4} \tag{6}$$

Due to the viscoelastic characteristics of samples, both the measured and sample stiffness and moduli are in the complex form, while the fixture tool only has the real part value by assuming the tool material is purely elastic.

So the machine or tool compliance (J_{tool}) can be simply expressed as

$$J_{tool} = \frac{1}{K_t} \tag{7}$$

Substituting Equation (5) and (7) into (4) gives

$$G_s^* = \frac{G_m^*}{1 - \frac{J_{tool}}{k_g} G_m^*} \tag{8}$$

Where G_s^* and G_m^* are the sample complex modulus and the measured complex modulus respectively.

For the parallel plate geometry, the sample complex shear modulus is

$$G_s^* = \frac{G_m^*}{1 - J_{tool}\, G_m^* \frac{\pi R^4}{2h}} \tag{9}$$

The Equation (8) can be rewritten in the form of storage and loss moduli as

$$G_s^{'} + iG_s^{"} = \frac{G_m^{'} + iG_m^{"}}{1 - \frac{J_{tool}}{k_g}\left(G_m^{'} + iG_m^{"}\right)} \tag{10}$$

By rearranging Equation (10), the storage ($G_s^{'}$), loss ($G_s^{"}$) moduli and phase angle (δ_s) of the sample can be calculated as

$$G_s^{'} = \frac{G_m^{'}\left(1 - \frac{J_{tool}}{k_g} G_m^{'}\right) - \frac{J_{tool}}{k_g} {G_m^{"}}^2}{\left(1 - \frac{J_{tool}}{k_g} G_m^{'}\right)^2 + \left(\frac{J_{tool}}{k_g} G_m^{"}\right)^2} \tag{11}$$

$$G_s^{"} = \frac{G_m^{"}}{\left(1 - \frac{J_{tool}}{k_g} G_m^{'}\right)^2 + \left(\frac{J_{tool}}{k_g} G_m^{"}\right)^2} \tag{12}$$

$$tan(\delta) = \frac{G_m^{"}}{G_m^{'}\left(1 - \frac{J_{tool}}{k_g} G_m^{'}\right) - \frac{J_{tool}}{k_g} {G_m^{"}}^2} \tag{13}$$

The geometry constant or geometry conversion factor k_g for the commonly used rheometer fixture geometry is listed below:

For parallel plate, k_g was shown in Equation (6).

For cone and plate,

$$k_g = \frac{3}{2\pi R^4 \emptyset} \quad (14)$$

Where R is the plate radius and ∅ is the cone angle.

For concentric cylinders or bob-cup geometry,

$$k_g = \frac{R_c^2 - R_B^2}{4\pi L R_B^3 R_c^2} \quad (15)$$

Where R_C , R_B is the radius of the cup and bob respectively and L is the bob length.

A2. INSTRUMENT COMPLIANCE MEASUREMENT AND CALCULATION

A2.1. *Scope:*

A2.1.1. This procedure is used to measure instrument compliance for DSR's.

A2.2. *Procedure:*

A2.2.1. Prepare the DSR in accordance with Section 8 of this standard using 4 mm parallel plates and allow approximately the plates to come to room temperature (approximately 20 minutes). Insure that any compliance correction values in the instrument software are set to zero.

A2.2.2. Apply a drop of SuperGlue™ (cyanoacrylate or any other type of super glue) to the center of the lower plate.

A2.2.3. Close the gap by moving the movable plate to form a thin layer (about 0.05 mm) of super glue between two plates. Ensure the thin layer of super glue film between plates is uniform.

A2.2.4. Clean up the extra super glue with a dry paper towel.

A2.2.5. Allow for sufficient time to fully cure the super glue (approximately 3 hours). Monitor the normal force as the cyanoacrylate will have a slight volume loss as it cures. Adjust the gap as necessary to maintain a normal force of 0 N.

A2.2.6. Perform a strain or stress sweep test at a frequency 1 rad/s.

Note 4—The strain/stress ramping range depends on the measuring system geometry (specifically the parallel plate radius) and the rheometer limits. Small strains and stresses are strongly suggested to avoid damaging the torque transducer. Start out at the lowest possible strain or stress achievable by the instrument and increase the strain in small increments.

A2.2.7. Plot angle displacement (angular rotation) versus torque obtained from the strain/stress test, and the instrument compliance is the slope of the linear fit (as shown in Figure 1).

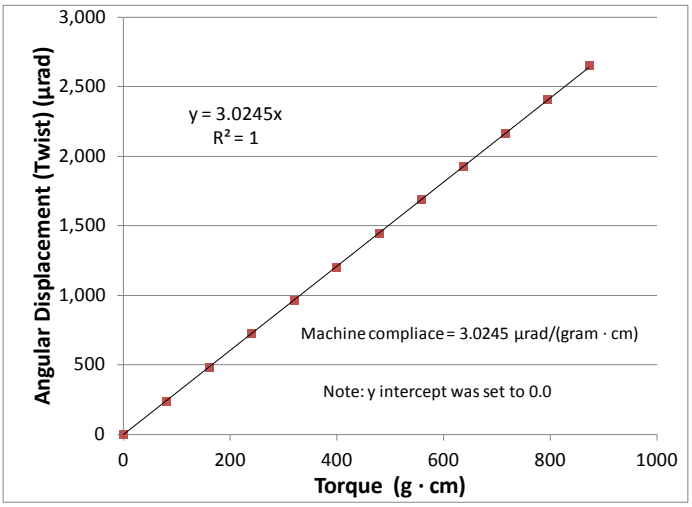

Figure 1—Example: Determination of Instrument Compliance from the Slope of the Linear Fit of the Angle Displacement and Torque Measurements

A3. DETERMINATION OF THERMAL EXPANSION OF THE MEASURING SYSTEM

A3.1. *Scope:*

A3.1.1. This procedure is used to measure the thermal expansion of the measuring system on DSR.

A3.2. *Procedure:*

A3.2.1. Mount the parallel plates onto DSR and leave the plates 1 mm apart.

A3.2.2. Heat the measuring system to 30°C and stabilize at this temperature for at least 30 min.

A3.2.3. Zero the gap using the normal force transducer and the instrument's "Zero Gap" function, and move the moveable plate so the plates are 1 mm apart. Lower the temperature to 20°C and condition for 20 minutes. Then move the moveable plate to the point where it just touches the fixed plate (indicated by a change in the normal force, note: the normal force should not exceed 10 g). The gap deviation from the zero position is the thermal expansion or change in length (ΔL) of the measuring system from the 10°C change in temperature (ΔT). The gap correction factor (g_α) of the system is

$g_\alpha = (\Delta L) / (\Delta T)$ (16)

where g_α = gap correction factor ($\mu m°C^{-1}$)
ΔL = gap change in length (μm)
ΔT = change in temperature (°C)

Repeat this measurement several times and determine the average gap correction factor.

A3.2.4. Adjust the gap when changing temperature to adjust for the thermal contraction or expansion of the system, e.g., assuming g_α = 2 μm $°C^{-1}$) then when changing from 30°C to 20°C the gap adjustment (Δh) is

(Δh) = g_α * (ΔT) = 2 μm/ °C * 10°C = 20 μm, i.e., the moveable plate is moved towards the stationary plate a distance of 20 μm.

A4. HOW TO DETERMINE m_r and G(t)

A4.1. *Scope:*

A4.1.1. This section provides an example of time temperature superposition (TTS) and master curve development of G'(ω) from the two frequency sweeps, interconversion from G'(ω) to G(t) and estimation of m_r and G(t) at 60 seconds from the G(t) master curve at the PG+10°C.

A4.2. *Definition of terms:*

A4.2.1. G'(ω) – Storage Modulus

A4.2.2. G(t) – Relaxation Modulus

A4.2.3. PG+10°C – Low Performance Grade temperature plus 10°C

A4.2.4. PG+20°C – Low Performance Grade temperature plus 20°C

A4.2.5. m_r(60 s) – slope of the relaxation modulus at a reference temperature of PG+10°C and 60 seconds

A4.2.6. G(60 s) – magnitude of the relaxation modulus at a reference temperature of PG+10°C and 60 seconds

A4.2.7. ω – Frequency (rad/s)

A4.2.8. a_T – Time-temperature superposition horizontal shift factor

A4.2.9. t – time (seconds)

A4.3. *Example:*

A4.3.1. A series of steps are involved when calculating the slope (m_r) and magnitude of the relaxation modulus G(t) from dynamic oscillatory shear data (frequency sweeps) at 60 seconds and a reference temperature of PG+10°C. The first step is to generate a G'(ω) master curve at a reference temperature of PG+10°C.

Plot the two frequency sweeps determined in Section 1. A typical representation of test data is shown in Figure 2. Fit the PG+10°C frequency sweep with a second order polynomial.

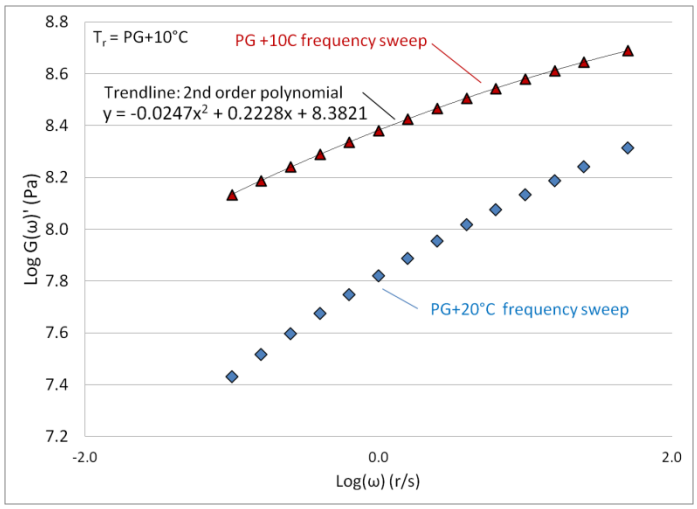

Figure 2—PG+10°C and PG+20°C Frequency Sweeps from Section 11, Procedure

A4.3.2. Use Excel™ solver to determine the horizontal shift factor (a_T) to translate the PG+20°C frequency sweep along the abscissa so that it overlaps the PG +10°C frequency sweep. The horizontal translation is accomplished by multiplying the PG+20°C frequencies by a_T and plotting the storage modulus as a function of the multiplied frequencies. The basis for the shift factor is known as time-temperature superposition (TTS). Table 2 demonstrates the calculation of the shift factor. To avoid error from extrapolation of the 2nd order polynomial, only G'(ω) data that approximately overlap are used to estimate a_T.

Table 2—Estimating the Horizontal Shift Factor a_T using Excel™ Solver

Least squre difference (LSD) (log G' freq. sweep — calculated log G' based on 2nd order polynomial)^2

Solver—changing cell

ω (r/s)	log ω (r/s)	G' from PG+20°C ω sweep (Pa)	log G' (Pa)	Shift factor = 0.0103	a_T * ω (r/s)	log (a_T * ω) (r/s)	log G' (2nd order polynomial) from figure 1) (Pa)	LSD
3.98	0.60	1.04E+08	8.02	Sum LSD = 7.93E-06	4.08E-02	-1.39	8.02	3.26E-06
6.31	0.80	1.19E+08	8.08		6.47E-02	-1.19	8.08	1.72E-06
10.00	1.00	1.36E+08	8.13		1.03E-01	-0.99	8.13	3.60E-07
15.85	1.20	1.54E+08	8.19		1.63E-01	-0.79	8.19	1.91E-07
25.12	1.40	1.74E+08	8.24		2.58E-01	-0.59	8.24	1.58E-06
39.81	1.60	1.95E+08	8.29		4.08E-01	-0.39	8.29	2.19E-07
50.00	1.70	2.06E+08	8.31		5.13E-01	-0.29	8.31	6.03E-07

Solver target cell

A4.3.3. Using the a_T determined in section 20.2.2 shift the PG+20°C frequency sweep so that it overlaps the PG+10C frequency sweep. The process is illustrated in Figure 3.

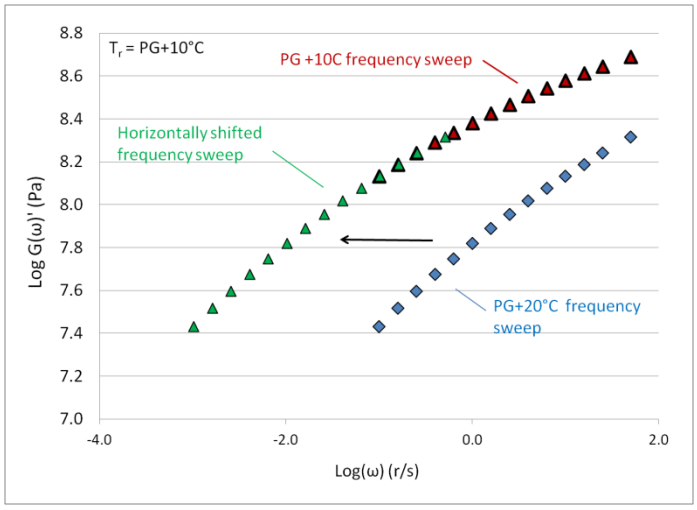

Figure 3—G' Master Curve at a Reference Temperature PG+10°C

A4.3.4. The relaxation modulus G(t) is then determined thru interconversion of the storage modulus *G'(ω)* by the approximate expression developed by Christensen (1982).

$$G(t) \approx G'(\omega)|_{\omega=2/\pi t} \quad (17)$$

Figure 4 shows the relaxation modulus determined using Equation 17. The relaxation modulus is fit with a 2nd order polynomial using the time points that bracket 60 seconds (0.78 to 2.78 in log scale) to generate the polynomial. The resulting 2nd order polynomial is

$$\log G(t) = -0.0366(\log t)^2 - 0.2195 \log t + 8.3311 \quad (18)$$

The slope of the relaxation modus at 60 seconds is determined by taking the first derivative of the 2nd order polynomial

$$\frac{d \log G(t)}{d \log t} = m_r = -0.0366 * 2 \log t - 0.2195 \quad (19)$$

Solve Equation 18 for G(60s) and Equation 19 for the slope, mr at 60 s.

G(60 s) = 66.85 MPa

m_r (60 s) = -0.35

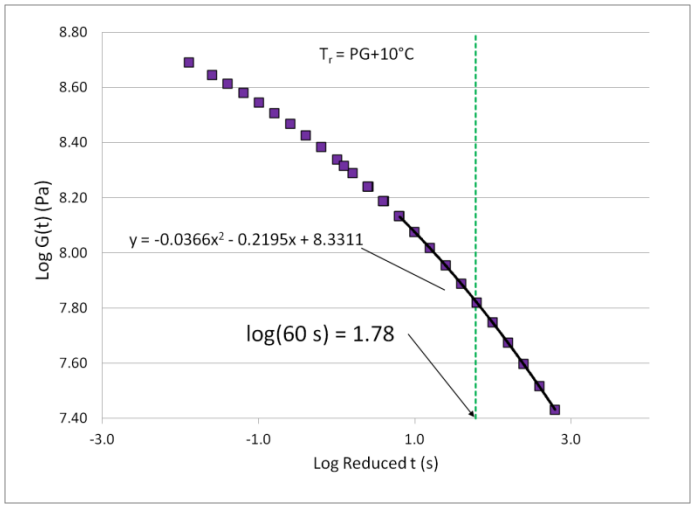

Figure 4—Relaxation Modulus Master Curve